Alma Mater Studiorum · Università di Bologna

SCHOOL OF ENGINEERING

SECOND CYCLE MASTER'S DEGREE in
ENERGETIC ENGINEERING

Graduation Thesis in
Sustainable Technologies for Energy Resources

Analysis of the effects of the external conditions on the hydrogen production by a mid-scale laboratory PEM electrolyzer

Candidate:
Marcello Savini

Supervisor:
Prof. Ernesto Salzano

Co-Supervisor:
Dr. Stefan Spitzer
Dr. Arnas Lucassen

Academic Year 2022/2023

Abstract

The aim of the work is to study the effects that external temperature causes on hydrogen production in a mid-scale laboratory PEM Electrolyzer. Specifically, various tests were carried out, which were identical to each other except for a variation in the external temperature, simulated in the laboratory using a dynamic climate chamber. After devising, testing and fine-tuning the experimental setup, the collected data were analysed from two points of view: i) the factors that, through a change in temperature, influence the efficiency of the electrolyser and ii) the qualitative analysis of the produced gas.

In particular, as temperature is considered the primary parameter assumed to exert the most significant influence on cell degradation, and given a worn cell, it was anticipated that there would be a more frequent occurrence of gas crossover phenomena through the membrane. Consequently, an alteration in the quality of the generated gas was expected to be observed.

Test results indicate that the impact of external conditions cannot be disregarded in the cell's energy consumption and deterioration processes. Nevertheless, no substantial evidence of notably significant pollutants was found in the generated hydrogen, nor were there any substantial alterations in gas quality observed. As the operating temperature varied, the sole noticeable change was an increase in the amount of water carried by the gas. Importantly, water is not properly a pollutant and can be more or less treated in subsequent drying processes, depending on the intended future utilization of the hydrogen. Finally, the discussion concluded with some considerations on the optimisation of certain setup components and the effectiveness of the start-up method used.

Contents

List of Figures

List of Tables

Chapter 1

Introduction

Today's world is in the process of an energy transition.
The utilization of fossil fuels irrefutably led to significant technological advancement in a short time span but, one of the major downsides is increasing pollution on such a scale, that the Earth couldn't withstand anymore without considering consequences. Presently these negative effects are visible in many forms and the most notable ones being connected to climate change. The Energy Institute (EI) Statistical Review of Worlds Energy report of 2023, saw a global primary energy demand increased by 1% in 2022, exceeding the 2019 pre-COVID level around 3% [1].

In order to achieve the EU's climate neutrality by 2050 [2], according to several studies conducted by the European Commission, the electrolysis of water has been acknowledged as a pivotal process with significant potential for decarbonization, especially when implemented in large-scale technologies. In the face of a progressively intermittent renewable energy generation, hydrogen produced through water electrolysis—owing to its exceptional purity and high specific energy—stands out as a paramount green alternative to current energy carriers. This is crucial to address the escalating energy demand and enhance grid stabilization efforts [3, 4, 5].

Today, Proton Exchange Membrane Water Electrolysis (PEMWE) technology demonstrates commendable performance, showcasing a high rate of hydrogen production and energy efficiency that aligns favorably with the standards set by cutting-edge systems in use today. When compared to other water electrolysis (WE) technologies, such as Alkaline Water Electrolysis (AWE) and Solid Oxide Water Electrolysis (SOWE), PEMWEs offer a range of advantageous characteristics. These include simplicity in operation, remarkable responsiveness to power fluctuations (making them ideal for pairing with non-programmable renewable energy sources), and the potential for compact design. However, there are still certain limitations that hinder the widespread adoption of this technology for large-scale applications. The primary limitations are linked to the substantial initial capital investment attributed to the inclusion of precious group metals (PGM) as Electrocatalysts, the utilization of Perfluorinated Sulfonic Acid (PFSA) membranes, and the costly bipolar plates. Only when the investment expenses decrease to the range of $300 - 500$ €$/kW$,

will PEMWE become a competitive choice for extensive large-scale applications. Furthermore, it is imperative to enhance the durability of PEMWE while minimizing efficiency loss. This is crucial to effectively lower maintenance costs and ensure alignment with the expected operational lifespan of around 100,000 *hours* [6]. Regarding this aspect, within the industrial community, a degradation rate on the order of 2-10 $\mu V \cdot h^{-1}$ is commonly accepted $\mu V \cdot h^{-1}$ [7]. Among the factors leading to a higher degradation rate, there are: i) The harsh environmental conditions, characterized by strong acidity and the presence of a high overpotential. ii) Material choices. iii) Operating conditions encompassing pressure cycles, load cycles of current density, and variations in working temperature.

A substantial segment of the scientific community is presently dedicating its efforts to researching the aging mechanisms that impact cell components, particularly in the context of intermittent power sources through reduced-scale investigations. An intermittent energy source indeed triggers a sequence of fluctuations that influence not only the quantity of hydrogen produced, but also parameters like pressure, operational voltage, gas purity, temperature, and subsequently, the degradation rate of the materials. Therefore, the entire system must be ensured [8].

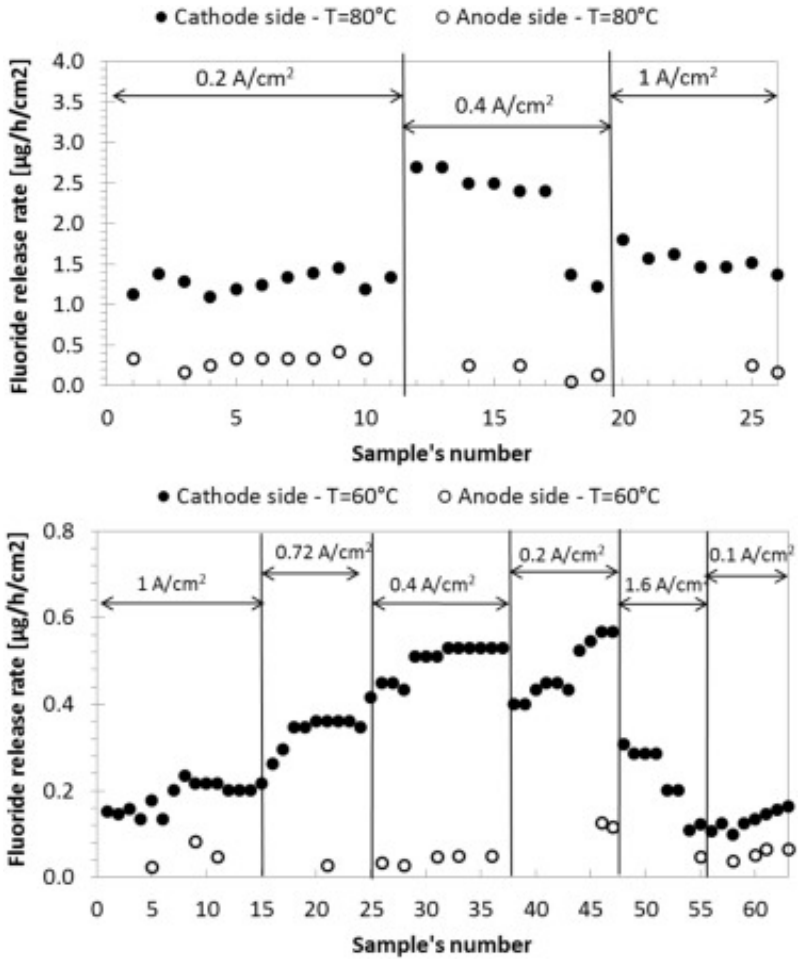

(a) Fluoride-ion at 353 and 333 K for different current densities

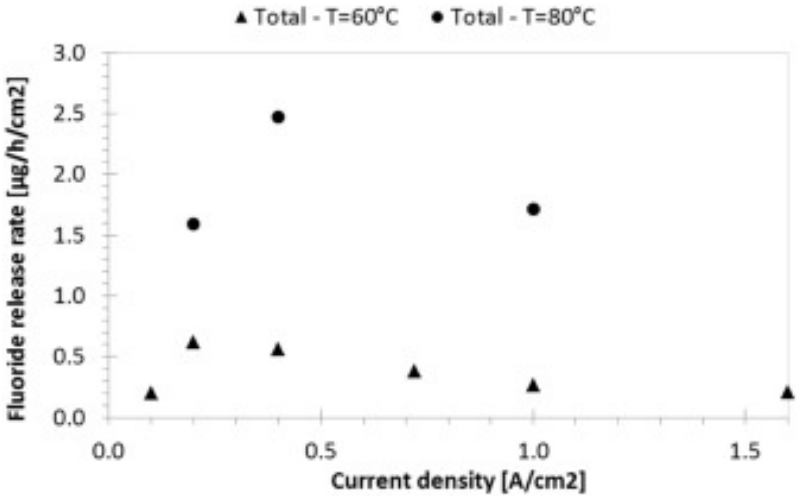

(b) Total mean fluoride-ion release rates depending on the current density

Figure 1.1: Fluoride-ion release rates, reported from [9]

One of the major issues in these scenarios is gas crossover. At times, these fluctuations exhibit gradients so pronounced that the crossover of oxygen and hydrogen, occurring respectively at the cathode and anode, cannot be dismissed, posing a significant challenge to inherent safety. This phenomenon becomes particularly evident during periods of low current load as reported by [9, 10] and shown in figure 1.1.

The concurrent presence of these persistent variations over time underscores the need for a comprehensive scrutiny of each parameter at play. Furthermore, when taking into account operational limitations like the minimum power load, the electrolyzer must cease operation if the electric power drops below the specified operational range. Indeed, within the auxiliary system, a pressure swing adsorption dehumidification unit displayed the greatest energy loss, followed by the energy loss in the AC/DC conversion unit. This implies that renewable energy cannot be harnessed during shutdown periods. Even if low power load operation is possible, the entire system will experience a notable decrease in overall efficiency.

Today's focus is on the study of system configurations and operating conditions, there is a need to understand the fluctuation patterns of naturally intermittent power and the influences of fluctuations that accelerate the performance degradation of water electrolyzers, as these fluctuation patterns do not follow Gaussian distributions [11]. As reported by H. Kojima et al. [8], the feasibility of tracking power fluctuations and subsequent changes in device performance under different stack temperature and pressure conditions is supported in most of the reviewed publications. However, some essential parameters, in particular the hydrogen purity and the electrolysis efficiency of a system incorporating auxiliaries, have not been well reported in most of the investigations, thus, it is not possible to compare fairly the electrolyzer performances among the methods.

Since the electrolysis of water is an endothermic reaction (in which a higher than theoretical voltage is required due to overpotential and ohmic losses) an electrolyzer

increases its operating temperature over time even when constant grid energy input is used. According to Ursúa et al. [12] on an AWE, transient operation results in a significant temperature increase for high energy production and a subsequent temperature decrease for low energy production. Furthermore, gas crossover caused safety problems by reaching relatively high concentrations when the amount of gas generated decreased with low energy production. Sanchez et al. [13] observed that a mere 5% increase in temperature led to a 4% rise in Hydrogen to Oxygen content and vice versa. Therefore, the fluctuations changed the state of the electrolyser and the purity of the generated gas.
Similar studies have been conducted for PEM technology, and part of the research is also aimed towards modelling the behaviour of these electrolyzers when driven by an unprogrammed, hence intermittent, renewable energy source.

1.1 Temperature Effects

As reported by Long Phan Van et al. [14] in a review article about sizing techniques, operating strategies, progress and challenges, most of the studies on direct photovoltaic-electrolyser coupling mainly focus on optimising this integration in order to maximise the Solar To Hydrogen (STH) factor. Often based on laboratory tests conducted under pseudo-ideal conditions, using models that depend on purely theoretical equations that tend to consider only the electrical coupling between the two technologies, completely neglecting or over-simplifying the thermal model, which may not accurately represent the system in different operation conditions. Besides, these tests are often carried out over a relatively short period of time, typically from a few hours to a few weeks. In contrast, the evaluations employed today to gauge cell quality and potential, along with the emerging Accelerating Stress Test (AST), extend over significantly longer duration, often surpassing 1000 hours of continuous operation [15, 16].

Not many studies delve into the influence of operating temperature and the environmental conditions that can affect it. In most cases, external conditions such as temperature and irradiation are only taken into account for the photovoltaic model [17, 18], since it is widely known that temperature has a considerable impact on its performance. Conversely, the electrolyser is often treated in an overly simplistic manner, considering it to be operating at a constant temperature or with discrete variations between an operating temperature and a cold start temperature [19], without adequately modelling the influence of the surrounding environment on it. Only a limited number of research publications have provided a laboratory-validated thermal model for electrochemical cells that avoids assuming a constant operating temperature, typically achieved by controlling the supplied water. Specifically, one such study [20] explored the thermal dynamics of an Alkaline Water Electrolyzer (AWE), while another study [21] investigated a Proton Exchange Membrane Water Electrolyzer (PEMWE), which, however, in the working temperature model does not take into account the temperature of the water entering the cell, a term that may vary in relation to atmospheric conditions in simpler systems.

The electrolyzer's voltage is significantly influenced by temperature.
When operating at lower temperatures, the electrolyzer requires more power to produce hydrogen, leading to a reduction in efficiency. This is because the activation overvoltage increases with decreasing temperature. However, for low overvoltages, increasing the temperature also increases the exchange current density, which can reduce the activation losses [22] and improve the efficiency of the electrolyzer. Additionally, elevated temperatures lead to diminished resistive losses [13, 23] and a lower reversible voltage.
The benefits of lower ohmic losses outweigh the negative influence of temperature, and therefore, an increase in temperature is considered to have a positive impact on the electrolyzer's voltage [23].

To enhance the catalytic effects and achieve high electrolytic efficiency, maintaining an elevated temperature is typically essential for the electrolytic cell. Chandesris et al. investigation, as reported in [9], provides insights into the time-dependent changes in membrane thickness, represented as a percentage of its initial value, when a Proton Exchange Membrane Water Electrolyzer (PEMWE) cell operates at $1A/cm^2$ under two different temperatures, $333K$ and $353K$. Their findings reveal that during the electrolysis process, regardless of the driving conditions, there is a continuous crossover of gases between the anode and cathode sides of the cell. The rate of permeation increases with rising temperature but decreases with higher current density. Notably, the crossover rate is significantly higher for Hydrogen-To-Oxygen (HTO) compared to Oxygen-To-Hydrogen (OTH).

In a separate thermal stress test conducted by Albert et al. [24], the membrane was immersed in $90°C$ water for a period of 5 days, resulting in a substantial increase in crossover gases. As anticipated, operating at elevated temperatures significantly reduces the membrane's lifetime. The studies identifies a maximum temperature of $80°C$ as the optimal compromise between minimizing membrane consumption and achieving the highest efficiencies [25].

1.2 The Crossover question

Jian Dang et al. [26] showed that Hydrogen diffusion in the Oxygen path is affected by temperature, gas partial pressure and diffusion coefficient. The increase in cathode pressure bought a rapid increase in hydrogen concentration in oxygen gas, which can be suppressed by increasing the current density. Platinum plating of the anode Porous Transport Layer (PTL) is also reported to reduce the hydrogen concentration in oxygen gas by re-oxidizing the crossed hydrogen gas to water, but it did not contribute to the improvement of the current efficiency.

Although most research has focused on studying hydrogen crossover, both for reasons of process efficiency and because hydrogen is more likely to permeate for dimensional reasons, in their studies Trinke et al. [27] and Martin et al. [28] showed that: i) Oxygen in Hydrogen fraction is higher at small current densities, decreasing with increasing current

density and is almost constant at higher current densities. ii) The cathodic oxygen outlet flux increases linearly with increasing current density. iii) The strong increase in Oxygen permeation might be related to the increasing supersaturation of dissolved Oxygen within the anode catalyst layer with increasing current density. iv) The cell using PGM Catalyst with high (ORR) Oxygen Reduction Reaction (Pt/C and IrO_2) showed the lowest oxygen content, consequently the major part of permeated oxygen recombines with the evolving hydrogen. However both the studies were conducted at constant temperature.

1.3 Statement of work

The described consequences of temperature and power fluctuation are shown by the flow chart in figure 1.2. Since the degradation attributed to power intermittency is not entirely clear from an electrochemical point of view, some studies have found that continuous operation exhibits the same or even more degradation than dynamic operation. For that reason the aging mechanisms cannot be attributed to a highly dynamic process [16, 29], but might be linked to mechanical stress caused by temperature and pressure variations.

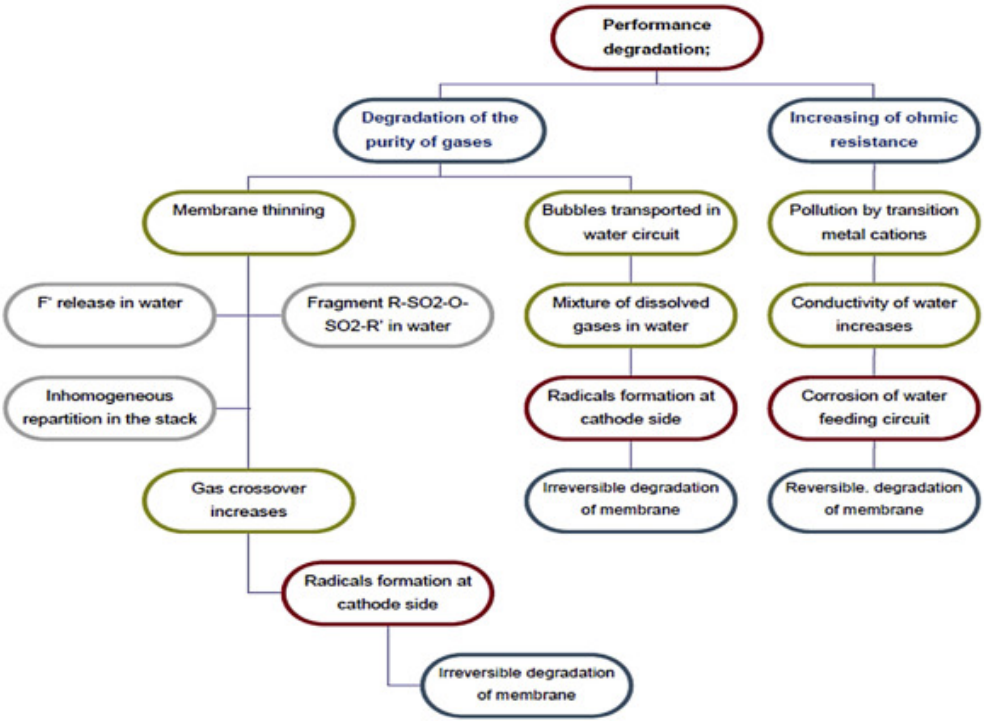

Figure 1.2: Performance losses mechanism related to membrane degradation. Red boxes: observable change; Green boxes: physical phenomenon; Grey boxes: physical consequences; Blue boxes: observable consequence, reported from [10]

Slower dynamics introduced by temperature and pressure play a more important role in their integration with solar energy. The limitations for the electrolyzers when operating in variable mode, are mainly due to the operating limits of the electrolyzers, especially regarding the minimum operating limit required for safety operation. There is no clear

evidence of high degradation rate with a variable operation. Rather, the degradation effects can be caused by improper operation: higher current densities, frequency shut-off, start-up and keeping the stack at open-circuit voltage. In this respect, intermittency rather than variability play a more relevant role in limiting the integration of electrolyzers with renewable energy [30].

The influence of the external temperature on the proper functioning of the cell is of fundamental importance, especially for systems that operate with renewable energy inputs, which are therefore not programmable. Furthermore, there is a lack of published studies in the literature concerning: i) the variations in efficiency, ii) the cell operating temperature iii) the quality of the produced hydrogen and the consequent impact on component consumption in the face of varying (or extremely low) external temperatures during low input power. In conclusion, for the construction of the test and its importance, as suggested by [14] and initially analysed by [31] certain considerations will be made regarding the cold-start of the electrolyzer.

The next chapter provides a brief introduction to hydrogen and a discussion of the fundamentals of electrolysis, highlighting respectively, its basic properties and focusing on PEMWE technology. The description of the setup and and the reasons for using each component are given in Chapter 3. In Chapter 4, the experimental results are explained. Finally, in Chapter 5, Conclusions and Remakes are discussed.

Chapter 2

State of the art

2.1 Hydrogen Fundamentals

Hydrogen is the first element in the periodic table with the atomic number 1. It is the lightest and most abundant element in the universe representing 75 % in mass or 90 % in volume of all matter. On Earth, it is mostly found in compounds with almost every other element.

In its free state, at atmospheric pressure and room temperature (298 K), it is in the form of a diatomic gas with the formula H_2 (dihydrogen), nonmetallic (except it becomes metallic at extremely high pressures), colourless, odourless, nontoxic, noncorrosive, tasteless (in principle, physiologically not dangerous) and highly flammable, with a boiling point of 20.27 K and a melting point of 14.02 K. In its bound state it is present in water 11.19 %, in all organic compounds and living organisms [32, 33].

Most of the hydrogen on Earth exists in molecular forms such as water and organic compounds but also exist as a free element in the atmosphere only to the extent of less than 1 ppm by volume, free ionic hydrogen is way more reactive than molecular hydrogen.

It plays a particularly important role in acid-base reactions because these reactions usually involve the exchange of protons between soluble molecules. In ionic compounds, hydrogen can take the form of a negative charge (anion) where it is known as a Hydride, or as a positively charged (cation) species denoted by the symbol H^+. The H^+ cation is simply a proton but its behavior in aqueous solutions and in ionic compounds involves screening of its electric charge by nearby polar molecules or anions.

There are three isotopes of hydrogen that can be found in nature, denoted ^{1}H, ^{2}H and ^{3}H. ^{1}H, ^{2}H are stable, while ^{3}H is radioactive, decaying into helium-3 through β-decay.

^1H (atomic mass 1.007825031898 Da) is the most common hydrogen isotope with an abundance of more than 99.98 %. Because the nucleus of this isotope consists of only a single proton, it is given the formal name protium.

^2H (atomic mass 2.014101777844 Da), the other stable hydrogen isotope, is known as deuterium and contains one proton and one neutron in its nucleus. It comprises $0.0026 - 0.0184$ % by volume of hydrogen samples on Earth, with the lower number tending

to be found in samples of hydrogen gas and the higher enrichment typical of ocean water.

Molecular hydrogen occurs in two isomeric forms: one with its two proton nuclear spins aligned parallel (orthohydrogen), the other with its two proton spins aligned antiparallel (parahydrogen). Parahydrogen is in a lower energy state than is orthohydrogen. At room temperature and thermal equilibrium hydrogen consist of approximately 75% orthohydrogen and 25% parahydrogen. When liquefied at low temperature, there is a slow spontaneous transition to a predominantly para ratio, with the released energy having implications on the storage.

2.2 Hydrogen Properties

Hydrogen can be considered an ideal gas over a wide range of temperatures and pressures (up to 10 MPa). At some point, however, like any other substance that is sufficiently cooled or compressed, it will act like a real gas. One of its most notable characteristics is its low volume-related density, which measures at 0.08987 kg/m^3 under normal temperature and pressure (NTP). This low density necessitates its compression or liquefaction for practical applications, as liquid hydrogen achieves a much higher density at approximately 70.8 kg/m^3 compared to its gaseous state.

Hydrogen gas is highly diffusive and highly buoyant; it is positively buoyant above a temperature of 22 K, that is almost over the whole temperature range of its gaseous state, and rapidly mixes with the ambient air upon release. The diffusion velocity is proportional to the diffusion coefficient and varies with temperature according to T^n (where n is in the range between 1.72 and 1.8). That's could be a favorable safety effect in unconfined areas, but it may cause a hazardous situation in (partially) confined spaces where the hydrogen can accumulate. Both diffusion and buoyancy determine the rate at which the gas mixes with the ambient air and the rapid mixing of hydrogen with the air is a safety concern, as it leads very soon to flammable mixtures, which on the other hand, for the same reason, also will quickly dilute to the non-flammable range.

As a fuel it represents a clean, environmentally benign energy carrier and as stated before, Hydrogen gas is highly flammable in connection with oxygen:

$$2H_2 + O_2 \rightarrow 2H_2O \tag{2.1}$$

Its enthalpy of combustion is indicated as a Lower Heating Value (LHV) of 242 kJ/mol (120 MJ/kg)or a Higher Heating Value (HHV) of 286 kJ/mol (141.865 MJ/kg) and can form explosive mixtures with air in a wide range of concentrations $4 - 74$ % and with chlorine at $5 - 95$ % [34, 35].

A stoichiometric hydrogen-air mixture, in which all the fuel is consumed at the time of the reaction, i.e. when the maximum combustion energy is released, contains 29.5 $vol\%$ hydrogen and the product of combustion is water vapour.

An explosive reaction can be triggered by a spark, heat or even sunlight alone. Its

self-ignition temperature (the temperature at which a flammable mixture can be ignited) is 858 K, which is relatively high but can be lowered by catalytic surfaces; moreover, the minimum ignition energy, i.e. the spark energy required to ignite the concentration of hydrogen most easily ignited in air, is at 0.017 mJ, much lower than that of hydrocarbon-air mixtures. A weak spark or electrostatic discharge, such as that of a human body, of about 10 mJ would be sufficient for ignition; this, however, is no different from some other burnable gases. The minimum ignition energy decreases further with increasing temperature, pressure or oxygen content.

The flame temperature of a mixture of hydrogen and air (stoichiometrically premixed) is at most 2403 K and emits ultraviolet light and in a mixture with a high oxygen content, it is almost invisible to the naked eye. The laminar burning velocity in a flammable gas mixture, defined as the speed at which a smooth, flat combustion wave advances in a stationary flammable mixture, is a gas property that depends on temperature, pressure and concentration.

The combustion velocity of hydrogen in air under stoichiometric conditions is 2.37 m/s, much higher than that of other hydrocarbon mixtures due to its rapid chemical kinetics and high diffusivity.

Phase at STP	Gas
Color	Colorless
Density	0.08988 kg/m^3 (NTP)
Melting Point	14.01 K
Boiling Point	20.28 K
Triple Point	13.8033 K
Critical Point	32.97 K
Heat of Fusion	0.117 kJ/mol
Heat of Vaporization	0.904 kJ/mol
Molar Heat Capacity	28.836 $kJ/mol.K$
Ionization Potential	13.5984 eV
Specific Heat	14.304 $J/g.K$
Thermal Conductivity	0.1805 $W/m.K$
Speed of Sound	1310 m/s

Table 2.1: Physical and Chemical Hydrogen Properties [32, 35, 36, 37]

The high combustion velocity of hydrogen increases the likelihood of a combustion transition from deflagration to detonation. Typically, the range of detonability falls within the interval of $18 - 59$ $vol\%$ of hydrogen concentration in air, expanding to $15 - 90$ $vol\%$ when in a pure oxygen environment. In such conditions, the detonation speed can reach values on the order of approximately 2000 m/s.

H_2 is nonreactive compared to diatomic elements such as oxygen. The thermodynamic basis of this low reactivity is the very strong $H - H$ bond, with a bond dissociation energy of 435.7 kJ/mol. The kinetic basis of the low reactivity is the non-polar nature of H_2 and its weak polarizability. It spontaneously reacts with chlorine and fluorine to form hydrogen

chloride and hydrogen fluoride respectively (both of which are poisons for the components of a PEMWE) and its reactivity is strongly affected by the presence of metal catalysts (such as PGMs). The most relevant physical and chemical properties are shown in 2.1

2.3 Hydrogen Energy

Although Hydrogen is the most abundant element in the universe, the existence of two hydrogen atoms (H_2) is scarce in nature which means hydrogen gas is not a direct energy source and needs to be produced. It is therefore important to disassociate it from various hydrogen-containing sources, where extraction needs to be carried out in an environmentally-friendly manner to produce pure hydrogen. Undeniably, this extraction process requires energy; nevertheless, its extraction can be performed employing any primary energy source as hydrogen is an energy carrier but not an energy source.

This indicates that a primary energy source among different candidates such as fossil fuels, natural gas, nuclear, solar, biomass, wind, hydro, or geothermal could be used to produce hydrogen. The diversity and range of alternative potential energy sources also make hydrogen a promising energy carrier.

While steam methane reforming remains a widely utilized but CO_2-intensive process for a substantial portion of current hydrogen production, it's worth noting that renewable electricity can be harnessed to conduct electrolysis processes [38], thereby enabling the production of green hydrogen with zero CO_2 emissions.

The cost of hydrogen production is a significant consideration [39]. Hydrogen production through steam reforming typically incurs a cost approximately three times higher per unit of produced energy compared to natural gas costs. Likewise, using electrolysis for hydrogen production with 5 $cents/kWh$ of electricity will cost somewhat beneath two times of natural gas-based hydrogen production cost.

Hydrogen fuel is dragging attention globally because of numerous reasons:

- Its production can be carried out using diverse energy resources;
- It is suitable to meet all energy requirements and can be employed in hydrogen fuel-cell vehicles, used for residential applications, used as an energy carrier, and can also be employed as a fuel for combined heating and power production systems;
- It is the slightest contaminating; subsequently, the hydrogen usage in fuel cells or combustion processes produces water;
- It is a flawless solar energy carrier.

A recent review article [40] conducted a comparative study and environmental impact assessment of nonrenewable and renewable sources based on hydrogen production approaches, in terms of Global Warming Potential (GWP), acidification potential, energetic and exergetic efficiencies, and production costs of mentioned methods. The results revealed that solar, wind, and high-temperature electrolysis were to be environmentally attractive while electrolysis-based conventional methods were least attractive comparing

the production costs. Consequently, efficiencies enhancement and cost reduction of wind and solar energy-based hydrogen production methods were found to be potential options.

According to the last European report regarding the productions method (and consequently consumption) of hydrogen [41], it's clear that on the total amount of its (estimated around 11.4 $Mt/year$), the mainstream production of hydrogen, around 95 %, comes from processing fossil fuels, specifically natural gas reforming, methane partial oxidation, and coal gasification. To meet the optimum outcomes, the selection of a suitable system with a source is also substantial. The outcome of using this approach is environmentally benign, clean, and sustainable hydrogen. Additional significant methods of producing hydrogen consist of water electrolysis and biomass gasification.

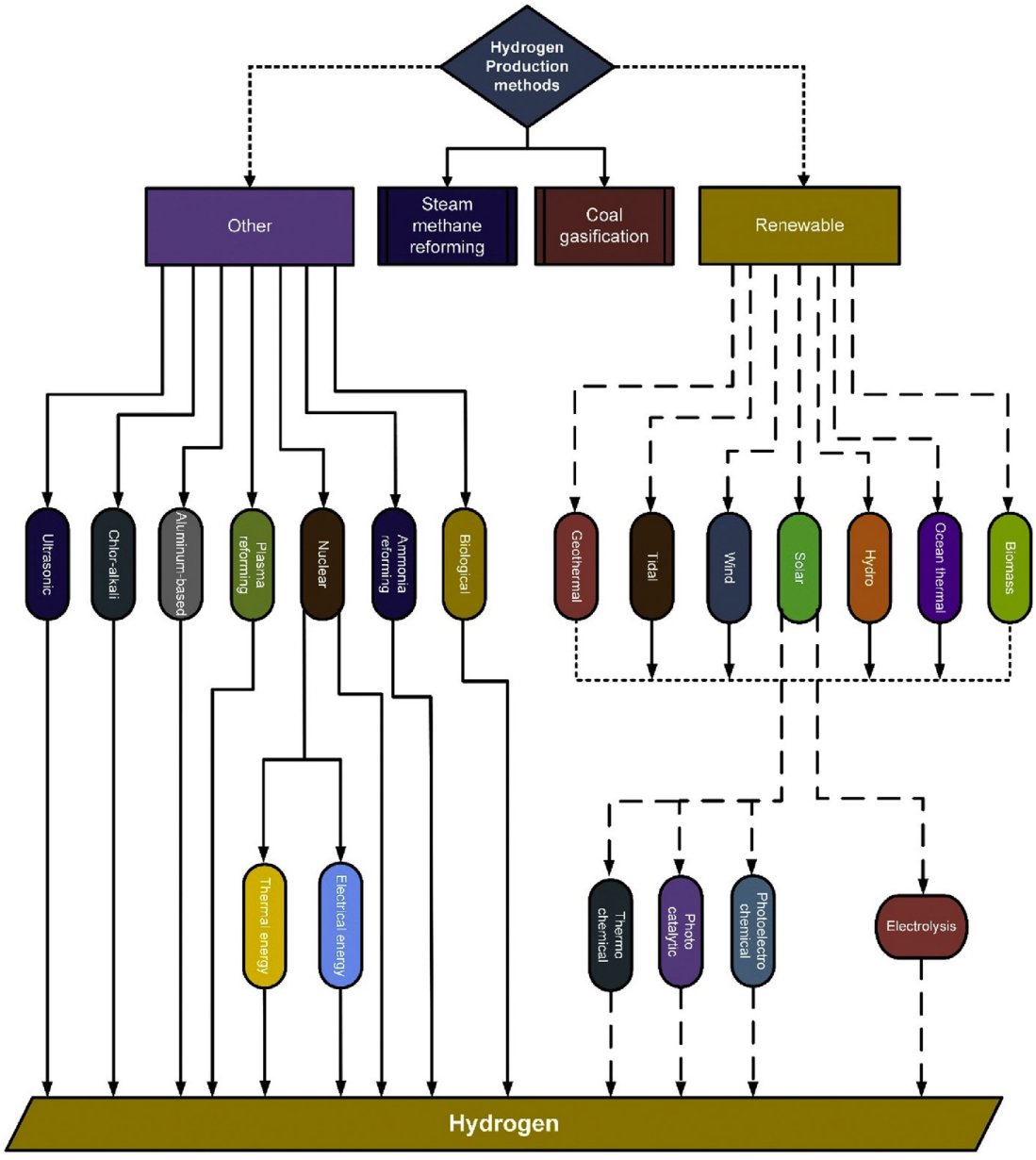

Figure 2.1: Hydrogen production methods

Hydrogen production methods are distributed between conventional (or dependent on fossil fuels) and renewable-energy categories. The significant conventional hydrogen production methods employing different sources are: i) Natural Gas Reforming, ii) Coal Gasification.

Renewable hydrogen production methods are gaining much attention because they offer clean, sustainable, and environmentally friendly energy solutions, overcoming the challenges of Greenhouse Gas Gmissions (GHE), fossil fuel depletion, and carbon taxes. The significant hydrogen production methods employing different renewable energy sources are: i)Water Electrolysis ii)Thermochemical iii)Photochemical iv)Geothermal v)Biomass

Fig. 2.1 exhibits the distribution of conventional and renewable hydrogen production methods. A brief description of the most meaningful methods is given below.

2.3.1 Hydrogen from Fossil Fuels

Compared with other fossil fuels, natural gas is the most suitable feed-stock for hydrogen production because of its wide availability and ease of handling. It also has the highest hydrogen-to-carbon ratio (4 to 1), which minimize the amount of CO_2 produced. Natural Gas (i.e. methane) can be converted into hydrogen by Steam Reforming, Partial Oxidation with oxygen or by combining both methods in the process of Auto-Thermal Reforming. Steam reforming is currently the preferred method, accounting for more than 50% of the hydrogen produced worldwide. In this process natural gas reacts with steam over a metal catalyst at high temperatures and pressures to form a mixture of carbon monoxide (CO) and hydrogen. Subsequently the reaction of CO with steam (water-gas shift) produces additional hydrogen and CO_2 as by-product (2.2). After purification, hydrogen is recovered, while the CO_2 is generally vented into the atmosphere.

Chemical Reaction	$\Delta H^0{}_{\mathrm{r,298\ K}}[kJ/mol]$	Name
$CH_4 + H_2O \rightleftharpoons CO + 3H_2$	206	Steam Reforming
$CO + H_2O \rightleftharpoons CO_2 + H_2$	-41	Water-Gas Shift
$CH_4 + CO_2 \rightleftharpoons 2CO + 2H_2$	247	Dry Reforming
$CH_4 \rightleftharpoons C + 22H_2$	75	Cracking (or Pyrolysis)
$2CO \rightleftharpoons C + CO_2$	-173	Boudouard Reaction

Table 2.2: Pattern of Reactions

Partial oxidation and auto-thermal reforming are more efficient then simple steam reforming, but require oxygen, whose separation from air at low cost is still difficult (and expensive).

As the importance of Natural Gas, also coal could supply a significant amounts of hydrogen. The technology to achieve this goal is the so called Integrated Gasification Combined Cycle (IGCC) that would allow the co-generation of hydrogen, electricity and therefore improve

the overall efficiency compared to the current commercial plants.

In this process coal is gasified by partial oxidation with oxygen and high temperature and pressure steam. The formed synthesis gas (mixture of CO, CO_2 and H_2) can be further treated with steam as in the above-mentioned reaction chain 2.2. Either way, because of its low hydrogen-carbon ratio, the coal releases much more CO_2. Producing hydrogen from petroleum oil, coal and natural gas is not attractive for the long run because it would not solve our dependence on fossil fuels and related environmental problems.

2.3.2 Hydrogen from Renewables

Electrolysis, the process of splitting water into hydrogen and oxygen using electricity, is an energy-intensive but well proven method to produce hydrogen:

It is currently more expensive than the production of hydrogen from fossil fuels, which explains its present less usage in the global hydrogen production. However it's the cleanest method to produce hydrogen with respect to greenhouse gas emission, as long as the electricity needed comes from renewable or nuclear energy sources.

With regards to this observation, one should bear in mind that hydrogen energy is only as clean and environmentally friendly as the process used to produce it.

The decomposition of water into hydrogen and oxygen at standard temperature and pressure is not favorable in thermodynamic terms, the power consumption at 100 % theoretical efficiency η_{th} is 39.41 $kWh/kg_{\mathrm{H_2}}$ [42]; however in practice is closer to $50 - 60$ $kWh/kg_{\mathrm{H_2}}$. Today current best processes for water electrolysis have an effective electrical efficiency of $70 - 80$ % but higher values can be obtained with more elevated water temperature or steam electrolysis. Since the efficiency of the electrolysis reaction is independent of the size of the cell, electrolyzers allow both centralized and decentralized production and, with the absence of moving parts, requires low maintenance[43].

Nowadays more than 60 % of the world's electricity is produced using fossil fuels, it would be unreasonable to use these to generate electricity for the purpose of producing hydrogen. To be sustainable electricity should be preferably derived from sources that do not emit CO_2 and pollutants such as SO_2 and NO_{x}.

Hydro-power is clearly well suited although its availability is limited, geothermal is a feasible approach in some geothermically active areas.
Today's challenges concern the exploitation of clean energies such as wind and solar generation. The discontinuous and intermittent production that characterises these two methods has limited their use to date as the electrolyser is not an ideal machine for operation at partial loads. Firstly, one would have a coupling that would never operate at full power, or at least, would do so for very short periods of time, and secondly, operation at discontinuous powers causes premature aging of the catalytic materials and the membrane, limiting their useful life.

2.3.3 Pro and Cons of Hydrogen energy

For what has been said so far about the properties and characteristics of hydrogen, it is possible to sum-up some positive and some negative aspects regarding its use as an energy carrier (and/or source).

Advantages of Hydrogen Energy

- **Renewable energy source and bountiful in supply**
  Hydrogen is a plentiful energy source for several compelling reasons, primarily owing to its abundant availability. While harnessing hydrogen may require significant resources, it stands as an essentially limitless resource, ensuring there is no risk of depletion. Electrolysis offers a means to extract hydrogen and oxygen from water. In this context, renewable energy sources can power electrolyzers, enabling the sustainable production of hydrogen from water. This approach creates a self-sustaining system independent of petroleum products, further emphasizing hydrogen's potential as a green and sustainable energy solution.
- **Practically a clean energy source**
  When hydrogen is burnt the by-products are totally safe, which means they have no known side effects and in particular, when consumed in a fuel cell, produces only water.
- **Hydrogen energy is non-toxic**
  This means that it does not cause any harm or destruction to human health, which makes it preferable to other energy sources such as nuclear power (nowadays not yet fully accepted by the public) and all fossil fuels ranging from coal to natural gas, whose imperfectly controlled combustion can produce toxic pollutants and/or cause harmful atmospheric events such as acid rain.
- **The Use of Hydrogen Greatly Reduces Pollution**
  When hydrogen is combined with oxygen in a fuel cell, electricity is produced, which can be used to power vehicles or drive an electric motor as a heat source and for many other uses. When it combines with oxygen, the only byproducts are water and heat, which is the advantage of using hydrogen as an energy carrier. The use of hydrogen fuel cells does not release carbon dioxide and other greenhouse gasses or other particulates when renewable sources such as water or solar energy are used in the production process.
- **More efficient than other sources of energy**
  As mentioned above about its properties, although characterised by a low volume density, hydrogen is definitely the energy carrier with the highest specific energy. Continued research and development of technologies that enable its storage at higher volume density will certainly make it the dominant energy carrier.

Disadvantages of Hydrogen Energy

Although hydrogen energy has many admirable and noble advantages, for most sectors it is still not the preferred solution yet. In its gaseous state, it is quite volatile. While this volatility gives it an advantage over other energy sources in terms of accomplishing many tasks, it also makes it risky to use and work with. Some of the disadvantages of hydrogen energy are as follows:

- **Expensive source of energy**
  Electrolysis in first place and steam reforming, the two main processes of hydrogen extraction, are extremely expensive compared to other forms of energy production. This is the real reason why hydrogen it is not heavily used across the world. Today, hydrogen energy is chiefly used to power most hybrid vehicles. A lot of research and innovation is required to discover cheap and sustainable ways to harness this form of energy and until then, hydrogen energy will remain exclusively for industrial process.
- **Storage and transport complications**
  One of hydrogen's properties, its low density, sets it apart. In fact, it's significantly less dense than gasoline, which has historically been the most energy-dense carrier readily storable. Consequently, to ensure its effectiveness and efficiency as an energy source, hydrogen must be compressed into a liquid state and stored at lower temperatures. Moreover, hydrogen's extreme lightness poses a challenge for transportation. Unlike oil, which can be safely transported through pipelines, or coal, which conveniently moves in dump trucks, the transportation of hydrogen is a complex undertaking. Handling it in large quantities presents formidable logistical hurdles, which is why, currently, hydrogen is primarily transported in small batches. These interactions with matter underscore the unique considerations involved in harnessing hydrogen as an energy carrier.
- **Not the safest source of energy**
  As mentioned the power of hydrogen should not be underestimated. Although gasoline is more dangerous than hydrogen, the latter is extremely flammable and often makes the headlines for its potential dangers. Compared to gas, hydrogen lacks smell, which makes any leak detection almost impossible and sensors must be installed.

2.4 Water Electrolysis

Water electrolysis is currently the most significant method for obtaining hydrogen from water without emitting polluting gases or depleting fossil or nuclear resources. It represents a fundamental process in electrochemistry, where a non-spontaneous red-ox reaction, characterized by a positive Gibbs free energy ($\Delta G > 0$), occurs upon the application of a direct electric current. This process enables the conversion of electrical energy into

chemical energy to split water. The hydrogen obtained through electrolysis can achieve the highest levels of purity, reaching up to $99.999 vol\%$, once the generated hydrogen has been properly dried and impurities have been removed. Such exceptional purity provides a substantial advantage over both fossil fuels and biomass-based processes, as electrolytic hydrogen could be directly supplied to fuel cells.

2.5 Electrolysis Fundamentals

Electrolysis of water is an electrochemical process in which electricity (electro-) is used to split (-lysis) water molecules into dissolved oxygen and hydrogen. Concretely, this electrochemical process involves reduction-oxidation (red-ox) chemical reactions. Specifically, it results in the production of hydrogen gas through the Hydrogen Evolution Reaction (HER) occurring at the cathode, and oxygen gas through the Oxygen Evolution Reaction (OER) occurring at the anode.

The process is performed by an electrolyser whose generic scheme can be fragmented in three levels as reported in Figure 2.2: i) The cell is the core of the electrolyser and it is where the electrochemical process takes place. It is composed of the two electrodes (anode and cathode) immersed in a liquid electrolyte or adjacent to a solid electrolyte membrane, two porous transport layers (which facilitate the transport of reactants and removal of products), and the bipolar plates that provide mechanical support and distribute the flow. ii) The stack has a broader scope, which includes multiple cells connected in series, spacers (insulating material between two opposite electrodes), seals, frames (mechanical support) and end plates (to avoid leaks and collect fluids). iii) The system level (or balance of plant) goes beyond the stack to include equipment for cooling/heating, processing the hydrogen, converting the electricity input (e.g. transformer and rectifier), treating the water supply (e.g. deionization) and gas output.

It operates by applying an externally generated voltage that must exceed the equilibrium voltage of water splitting, leading to the decomposition of water molecules. Electrons are generated (oxidation) at the anode, travel externally through an electrical circuit, and are consumed (reduction) at the cathode. It's important to note that this electron flow direction is opposite to the direction of current flow.
Regardless of the electrolyte type, the overall reaction of water electrolysis can be written as reported in equation 2.2.

$$2\,H_2O \rightarrow 2\,H_2 + O_2 \tag{2.2}$$

Water electrolysis does not occur spontaneously for temperatures below 2250 $^\circ C$ [33], it needs to be supplied with additional energy in the form of electricity and heat.

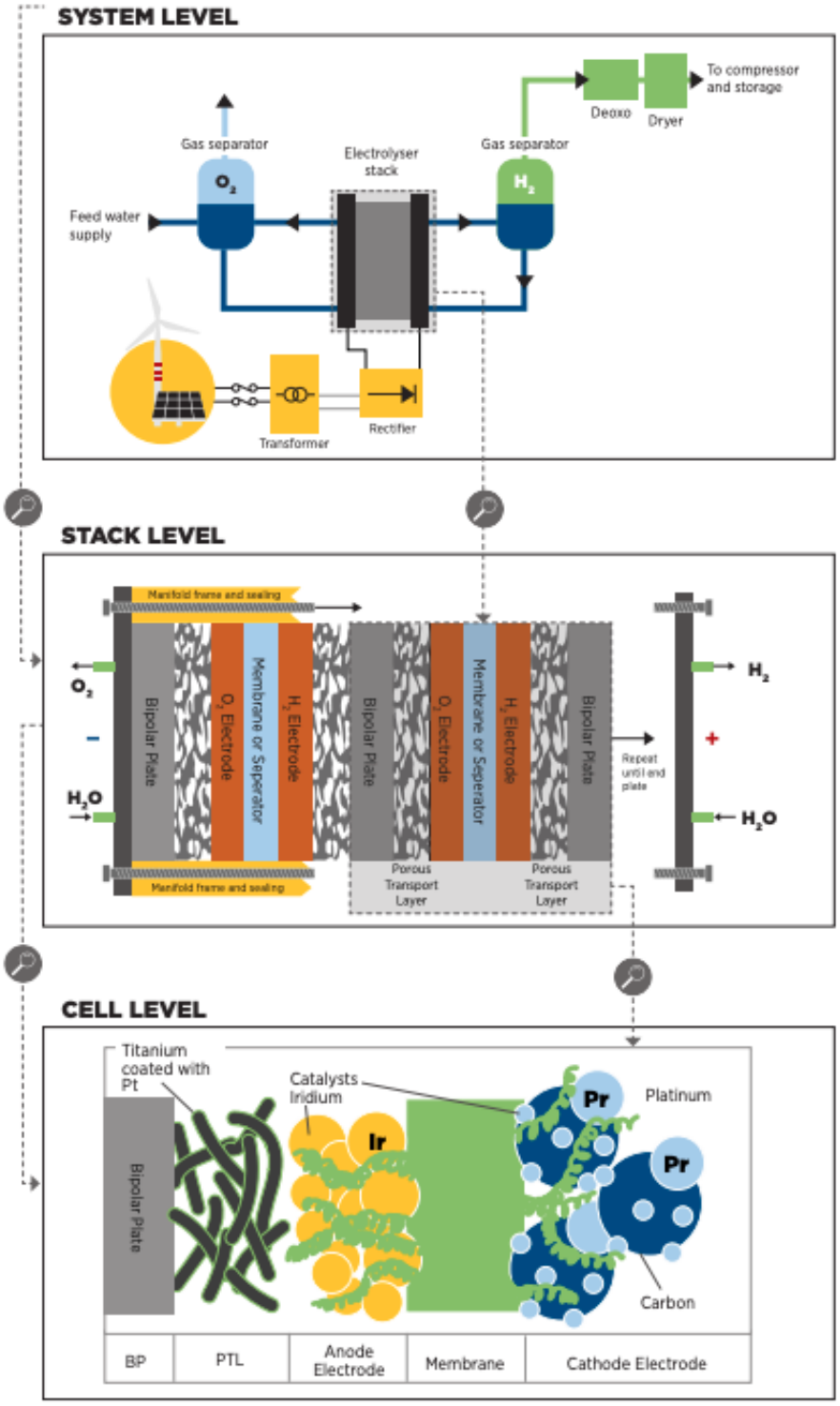

Figure 2.2: Basic components of water electrolyzers at different levels, reported from [44]

By looking at the enthalpy of reaction, defined as a change in enthalpy between the reactants and products ΔH $[kJ/mol]$:

$$\Delta H = \Delta G + T\Delta S \tag{2.3}$$

The entropy of the reaction products is higher than those of the liquid reactants, so $\Delta S > 0$. The term 'reaction Gibbs free energy' ΔG is therefore associated with the overall change in entropy and since a spontaneous process is associated with an increase in entropy, so ΔG is less than zero ($\Delta G < 0$), the electrolysis is a non-spontaneous process that requires work, which results in a positive value for ΔG ($\Delta G > 0$). It represents the maximum amount of work that can be obtained from the energy released in a reaction if ΔG is less than zero [33].

Under standard conditions (at a temperature of $298K$, pressure of $1atm$, and pH 0), the change in Gibbs free energy is denoted as ΔG^0 and is equal to -237.2 $[kJ/mol]$.

To perform this work, it is necessary to apply a potential, represented as U_0 (difference between the standard electrode potentials at the anode and at the cathode, measured under standard conditions), which is calculated as ΔG^0 divided by twice the Faraday constant $F = 96485.3321$ $[sA/mol]$:

$$U_0 = \frac{\Delta G^0}{2F} \tag{2.4}$$

resulting in an approximate value of $1.229V$.

This potential, known as the standard electrode potential, is temperature-dependent, as illustrated in equation 2.5 [45].

$$U_0 = 1.5184 - 1.5421 \times 10^{-3}T + 9.523 \times 10^{-5}T\log T + 9.84 \times 10^{-8}T^2 \tag{2.5}$$

In non-standard conditions, the equilibrium voltage U_{eq} is determined by U_0 and additional factors like temperature, concentrations, activities, or partial pressures of reactant and product species, as described by the Nernst equation 2.6.

$$\mathrm{U}^{Rev} = \mathrm{U}^0 - \left(\frac{R \cdot T}{n \cdot F}\right) \cdot \ln\left(\frac{\prod (a_{\mathrm{Rev}})^j}{\prod (a_{Ox})^k}\right) \tag{2.6}$$

Thermodynamically, at least $1.229V$ must be applied at the reaction to proceed but, because of energy losses due to resistance and irreversibility, also at higher voltages the heat generated by the current passing through the ohmic resistor turns out to be exactly that necessary for the endothermic reaction to maintain a constant temperature. The established potential:

$$U_{tn} = \frac{\Delta H^0}{2F} \tag{2.7}$$

known as thermoneutral voltage results in an approximate value of $\approx 1.48V$ by considering

$\Delta H^0{}_{\mathrm{r,298\ K}} = 285.83\ [kJ/mol]$.

Therefore to achieve a certain decomposition rate, the cell voltage U must exceed the thermoneutral voltage $U > U_{tn}$ and additionally the required electrode potential values to achieve specific rates or current densities strongly depend on the pH value of the electrolyte.

In general, electrodes involved in oxygen-evolving reactions tend to exhibit significantly higher overpotentials, especially when used in neutral or acidic conditions. This phenomenon occurs because it is easier to oxidize a negatively charged hydroxide ion compared to oxidizing a neutral species, as noted in the study by Fabbri et al. [46]. On the other hand, while hydrogen-evolving electrodes typically do not show significant overpotentials, their overpotential values tend to increase when used in an alkaline or neutral environment, as reported by Durst et al. [47]. This is because the HER demonstrates much lower overpotentials in an acidic environment, where it is simpler to reduce a positively charged proton than to reduce a neutral species.

With respect to the electrolyte used, the two possible electrolysis reactions (occurring at the cathode and anode respectively) are shown below:

In acid medium:

$$2\,\mathrm{H^+} + 2\,\mathrm{e^-} \rightarrow \mathrm{H_2} \tag{2.8a}$$

$$\mathrm{H_2O} \rightarrow 2\,\mathrm{H^+} + \frac{1}{2}\,\mathrm{O_2} + 2\,\mathrm{e^-} \tag{2.8b}$$

In alkaline or neutral medium:

$$2\,\mathrm{H_2O} + 2\,\mathrm{e^-} \rightarrow \mathrm{H_2} + 2\,\mathrm{OH^-} \tag{2.9a}$$

$$2\,\mathrm{OH^-} \rightarrow \mathrm{H_2O} + \frac{1}{2}\,\mathrm{O_2} + 2\,\mathrm{e^-} \tag{2.9b}$$

2.5.1 Oxygen Evolution Reaction

Several studies conducted by Hoare, Conway, Bard and others, as also reported in [48], showed that the necessary voltage to produce oxygen on a metal surface is related to the red-ox potential of the metal/metal oxide couple, this means oxygen cannot be released by the surface if the corresponding metal oxide is not formed.

The OER mechanism involves a four-electron transfer process, which necessitates a four step red-ox reaction to produce O_2. Therefore, OER tend to have slower reaction kinetics than HER, and this reaction rate often determines the overall performance of the energy conversion device.

Generally the accepted Adsorbate Evolution Mechanisms (AEM) that clearly describe the process are the Eley-Rydeal (ER)-type and the Langmuir-Hinshelwood (LH)-type as shown in Figure 2.3. A better overview in both acidic and basic mediums was carried out

by Matsumoto and Sato [49], including: the Yeager and Wade, Krasil Shchkov, Bockris [50] and Hackerman pathway along with the renowned electrochemical oxide and oxide pathway. The different reaction pattern are listed in the Appendix A

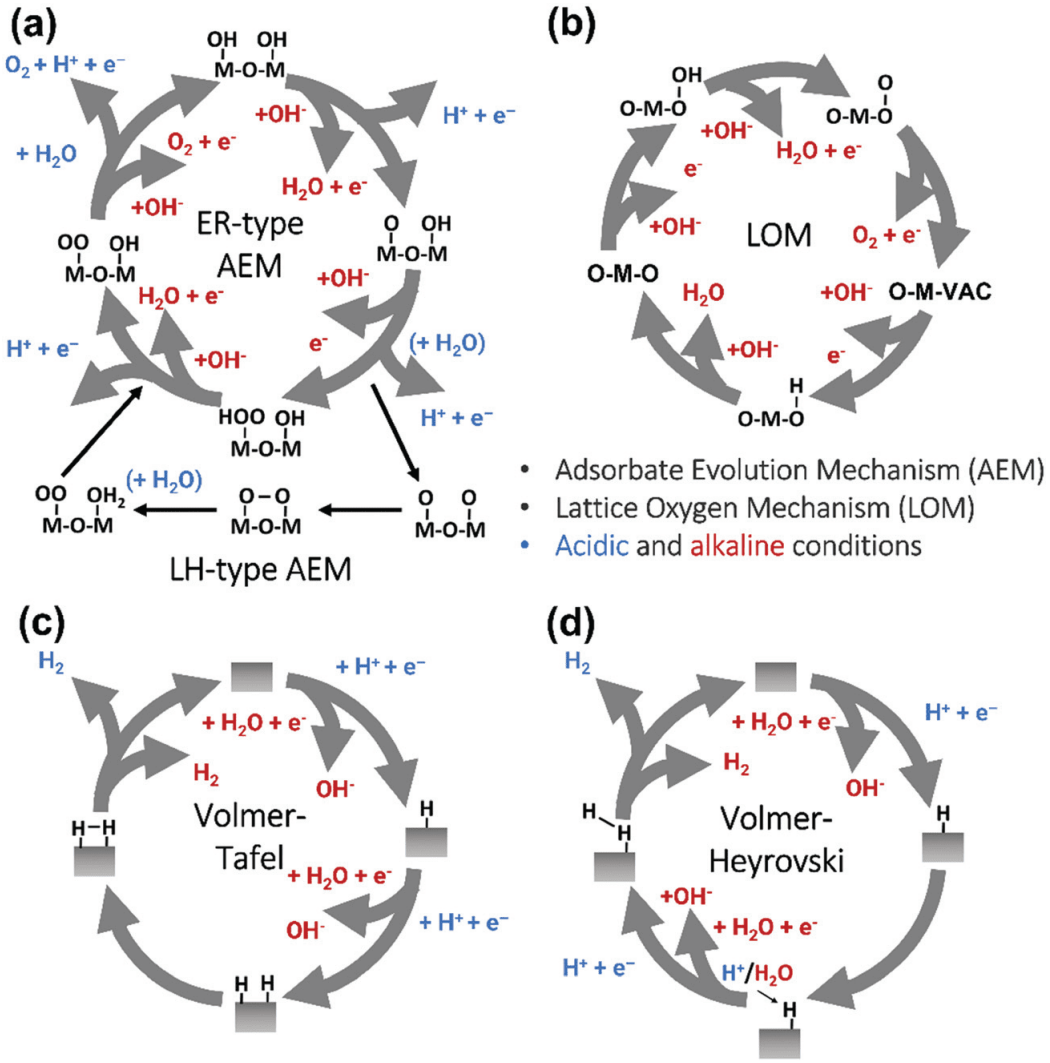

Figure 2.3: (a) The AEM of OER in the acidic (blue) or alkaline (red) medium. (b) The LOM of OER in alkaline medium. (c) The Volmer–Tafel HER mechanism in acidic (blue) or alkaline (red) conditions. (d) Volmer–Heyrovsky mechanism of the HER. Image reported from [48]

Regardless of whether the reaction takes place in an acidic or basic environment, the sequence starts with the formation of Metal Hydroxide intermediates (MOH) subsequently converted to Metal Oxide species (MO). Indeed, depending on the nature of the electrolyte, the Oxygen Evolution Reaction (OER) can follow two distinct pathways. Under acidic conditions, two MO centres react by splitting directly into dioxygen or an MO intermediate reacts with water. Under neutral or alkaline conditions, the two MO centres may react in the same way, either by splitting directly into dioxygen or by reacting with OH^- to form a hydroperoxide species, which subsequently decomposes, releasing dioxygen.

The ER-type AEM mechanism assumes active sites of a single metal cation; after the

formation of the metal intermediate compound in the active site, as a the second step, O^* binds with a water molecule to form OOH^*. In a subsequent third step, OOH^* oxidises further to become OO^*, which is then released as O_2.

The LH-type AE Mechanism, on the other hand, assumes two adjacent active sites of metal cations. Therefore, in the second step, OO^* is formed between two O^* species through the direct coupling of two adjacent surface metal sites [51].

Similarly, under alkaline conditions, ER-type AEM involves the evolution from OH^- reagent to OH^*, O^*, OO^* intermediates to the O_2 product on a single active metal site, whereas LH-type AEM assumes that two adjacent metal sites are involved.

It is important to emphasise that the performance of a specific OER depends on the nature of the catalytic material. From the volcano graph representing the O_2 production activity from the surface of first-row transition metal oxides (Figure 2.4), due to their excellent electrical conductivity and low redox potential, Ru and Ir noble metal oxides are at the top of the graph. The LH-type mechanism occurs mainly for Co-based catalysts [52] while the ER-type is reported for Ru-based catalysts [53].

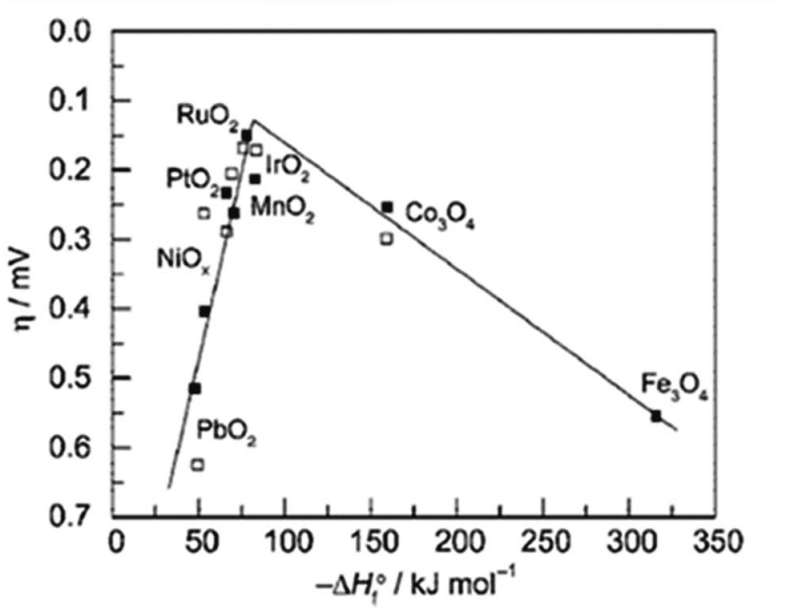

Figure 2.4: Volcano plot demonstrates the relationship between the rate of O_2 oxidation on transition metal oxide surfaces and change in enthalpy in acidic (black) and basic (white) solutions. Image reported from [54]

In general, the most active OER are RuO_2 and IrO_2 in both acidic and alkaline electrolysis, however: they are PGM-based materials i.e. scarce and expensive and they are not stable.

Therefore, new more stable materials have been developed, such as perovskites, bimetallic cobaltite oxy-/thio-spinels as well as $NiO_c - based$ electrocatalysts [55] which however show a different reaction path. The AEM no longer proceeds by proton-coupled electron transfer (PCET) but via non-concerted proton-electron transfer steps in a mechanism

called Lattice Oxygen Mechanism (LOM), where a structural change during the process lead to the formation of an oxy(hydroxide) surface layer that is highly OER-active [56], not covered in the following paper.

2.5.2 Hydrogen Evolution Reaction

The Hydrogen Evolution Reaction (HER) [57] has been the subject of extensive study in electrochemistry due to its relatively straightforward nature. Unlike the slow kinetics associated with the OER, the kinetics of the HER is significantly faster because of its simplicity. This allows the achievement of high current densities ($> 1\ A/cm^2$) with an extremely low overpotential [58, 59].

The reaction sequence for the HER initiates with the adsorption of either a proton in acidic conditions $M - H^+$ or a water molecule in neutral or alkaline environments $M - HOH$. This leads to the reduction of the adsorbed water molecule or proton, resulting in the formation of $M - H^*$ and the release of OH^- (in the case of the reduction of chemisorbed water). This initial phase takes the name of the Volmer step.

Subsequently, two distinct pathways can be distinguished: i) The combination of the chemisorbed hydrogen atom H^* with another chemisorbed hydrogen atom H^* leads to the chemical desorption of $H_{2,ad}$ (adsorbed hydrogen). ii) The electrochemical reaction of the chemisorbed proton H^+ with another proton or water molecule from the solution is followed by further electrochemical discharge and desorption of H_2.

The former sequence of steps corresponds to the Volmer-Tafel mechanism (chemical) [60], while the latter is known as the Volmer-Heyrovsky mechanism (electrochemical) [61], reported respectively in Figure 2.3. Between the two, the Tafel mechanism is more facile.

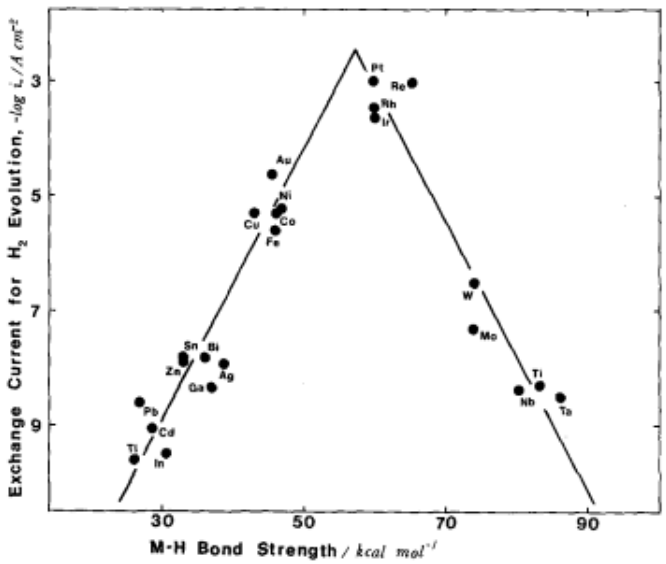

Figure 2.5: Exchange currents for electrolytic hydrogen evolution vs. strength of intermediate metal-hydrogen bond formed during electrochemical reaction itself. Image reported from [48]

The occurrence of either the Volmer-Tafel or the Volmer-Heyrovsky mechanism in the Hydrogen Evolution Reaction (HER) depends on various operating parameters that include: the pH of the solution, the electrode potential, and the specific nature and structure of the electrode being used, as previously highlighted for the Oxygen Evolution Reaction (OER).

Exchange current densities for the HER on pure metals in acidic environments have been extensively documented in numerous experimental studies, as comprehensively compiled and famously presented by Trasatti [62]. When these values are plotted against the strength of the metal-hydrogen bond, a characteristic pattern emerges known as the '*volcano*' curve as reported in Figure 2.5.

This pattern aligns with the Sabatier principle in fact the HER activity increases to a peak value at moderate bond strengths (e.g., Pt, Rh, Ir) and subsequently decreases as the bond strengths become higher. One can easily understand that the $M - H^*$ bond strength will influence the catalytic activity of metal towards the HER indeed a certain strength is needed to support the formation of the $M - H^*$ bond, but a too strong $M - H$ bonding is counterproductive because chemisorbed intermediates or product species will not be easily released from the surface.

2.6 Thermal Properties

Electrolyzers are often modeled under isothermal conditions to reduce the complexity of the model. While this simplification may be acceptable for steady-state operation, temperature-dependent properties are crucial for dynamic simulations. Typically, its thermal modeling 2.10 employs the thermal capacity C_{th} to provide thermal inertia to the system. The temperature variation also depends on the enthalpy flows entering and exiting the electrolyzer, as well as the thermal balance.

$$C_{th}\frac{\mathrm{d}T}{\mathrm{d}t} = \sum_i \dot{m}_i h_i + \sum_j \dot{Q}_j \tag{2.10}$$

The thermal capacitance of a subsystem is calculated by multiplying the respective masses of its constituent materials by their heat capacities, as defined in equation 2.11

$$C_{th} = \sum_k m_k c_{p,k} \tag{2.11}$$

Heat losses to the surroundings are described by thermal resistances, which account for the effects of surfaces with convective heat transfer coefficients, as defined in equation 2.13.

$$R_{th} = \sum_l (\alpha_l S_{th,l})^{-1} \tag{2.12}$$

Capacitances and thermal resistances are aggregated to the whole system according to the respective electrical circuit rules and their multiplication yields the thermal time constant τ_{th}

$$\tau_{th} = C_{th} \cdot R_{th} \tag{2.13}$$

This parameter quantifies the time it takes for a system to experience a 36.8% decrease in its initial temperature solely due to convective heat losses, without any additional heat input. Providing a temporal representation of the thermal system's characteristics and offering insights into heat capacity and heat losses.

2.7 Electrolysis assessment parameters

As mentioned in section 2.5, it is important to emphasise the factors and causes that impact the performance of an electrolytic process. Asha Raveendran et al. [63], according to Anantharaj et al. [64], reviewed the electrochemical parameters affecting the electrocatalysis of water splitting and electrocatalysts that could improve the performance of HER and OER.

Efficiency losses have distinct origins.
To gain a clearer insight into how these impacts the cell dynamics, a brief introduction to the most significant evaluation parameters, such as: the overpotentials, Tafel slope, Faradaic efficiency, etc... are given below.

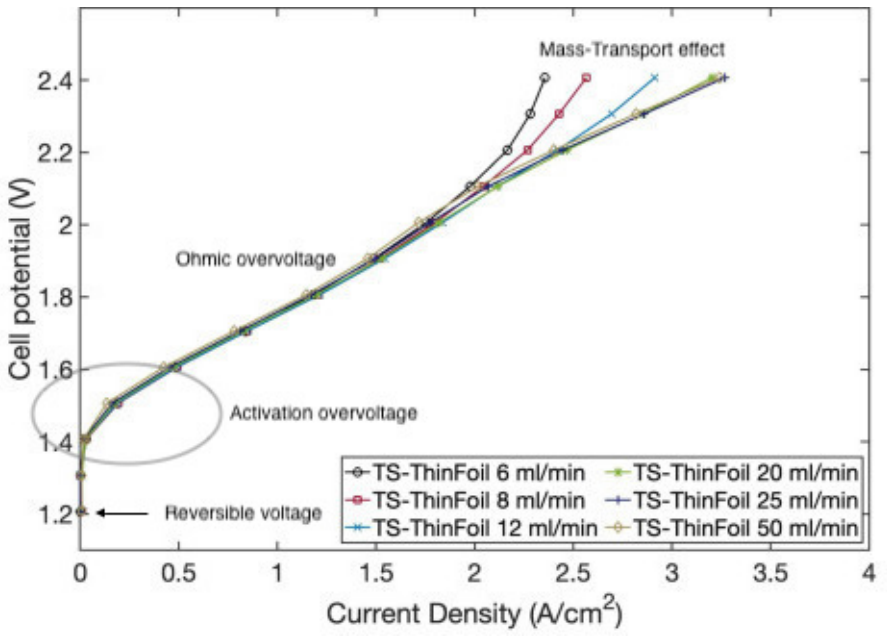

Figure 2.6: Overpotentials

2.7.1 Overpotentials

An overpotential is the potential beyond a reversible potential (respectively 0 and $1.229V$ for HER and OER) that produces an increased thermodynamic driving force for

the process and it is required to overcome the intrinsic kinetic hindrance in electrochemical water splitting. There are different types of overpotential arising from different nature *i.e.* activation, ohmic, concentration, bubble and Kinetic overpotential. These compete in their respective ways, as shown in the equation 2.14. A brief description of them is provided below and in order to better understand the effect these have on cell dynamics, the Figure 2.6 is used as an example.

$$U_{cell} = U_{rev} + \eta_{act} + \eta_{con} + \eta_{ohm} + \eta_{\Theta} + \eta_{diff} + \eta_{OER} \tag{2.14}$$

Activation overpotential

The activation overpotentials η_{act} occurring respectively at the anode and the cathode result from the additional potential required to overcome the energy barrier that hinders the initiation and acceleration of electrochemical reactions at the desired rate [65].

The Tafel equation can be used to calculate both the values:

$$\eta_{act,an} = a_{an} + b_{an} \log j \tag{2.15}$$

$$\eta_{act,cat} = a_{cat} + b_{cat} \log j \tag{2.16}$$

where a_{an} and a_{cat} are the constants of the Tafel equation, j is the current density in $[A/m^2]$, and b_{an} and b_{cat} are the Tafel slopes. The choice of an appropriate electrocatalyst could cause the decrease of these values.

Concentration overpotential

Concentration overpotential is caused by a rapid reduction in concentration at the interfaces due to concentration variance between ions in the bulk of the solution and on the electrode surface.

The effect of this term is accurately described by the Bulter-Volmer equation 2.17 [66]

$$\mathrm{j} = \mathrm{j}_0 \left[\exp\left(\frac{\beta n F}{RT} \eta_{con,an} \right) - \exp\left(-\frac{(1-\beta) n F}{RT} \eta_{con,cat} \right) \right] \tag{2.17}$$

where: $\eta_{con,an}$ and $\eta_{con,cat}$ are respectively the anode and the cathode concentration overpotentials, j_0 is the exchange current density which represents the rate of the electrochemical reaction at equilibrium conditions, β is the charge transfer coefficient (or symmetry factor), which characterizes the symmetry of the reaction with respect to electron transfer and it is related to the shape of the activation energy, n is the number of electrons involved in the reaction taking place at the electrode.

Under pure mass transfer control the expression can be written as

$$\mathrm{j} = \mathrm{j}_0 \left[1 - \exp\left(\frac{nF}{RT} \eta_{con} \right) \right] \tag{2.18}$$

with

$$\eta_{con} = \eta_{con,an} + \eta_{con,cat} \tag{2.19}$$

Ohmic overpotential

When current flows through the cell, it will also encounter resistive effects that increase the cell voltage such as the presence of electronic conductors on both sides of the electrode interface, etc... following the Ohm's law $\eta_{ohm} = iR$. The ohmic overpotential can be expressed as the sum of all these terms:

$$\eta_{con} = \eta_{bp} + \eta_{cc} + \eta_{gdl} + \eta_{MEA} + ... \tag{2.20}$$

Only for the PEM electrolyzer, the resistivity of the membrane depends strongly on its water content and temperature because most of the looses are caused by ionic conduction [67, 68], it is in fact widely known that electron transport is significantly faster than proton transport. With regard to proton transport across the membrane the overpotential can be write as:

$$\eta_{MEA} = i(x) \left(\frac{t_m}{k_m(x)} \right) \tag{2.21}$$

where x is the location in the membrane measured from the electrode-membrane interface, t_m is the thickness of the membrane and K_m is the conductivity of the membrane:

$$k_m(x) = i(x) \left(0.5139\lambda_m - 0.326 \right) \exp\left(1286 \frac{1}{303} - \frac{1}{T} \right) \tag{2.22}$$

with λ_m as the water content inside the membrane.

Bubble overpotential

During the electrolysis of water, especially at high current densities, the evolution of oxygen and hydrogen gas involves the formation, growth, detachment and transport of gas bubbles that cannot be avoided. These processes further increase voltage losses associated with both reaction kinetics and ion transport.

Bubbles that adhere to the catalyst surface reduce its effectiveness, while bubbles within the electrolyte increase ohmic losses related to ionic transport, a recent work carried out by Frida H. Roenning et al. [69] investigated that phenomena and suggested some solutions.

According one more time to the Tafel equation 2.24, the current density and therefore the overpotential obtained is reduced by a factor Θ representing the bubble coverage ratio on the catalyst surface $0 < \Theta < 1$.

$$i_\Theta = \frac{I}{A(1-\Theta)} \tag{2.23}$$

$$\eta_\Theta = a + b \log i_\Theta \tag{2.24}$$

Mass Transport overpotential

η_{diff} refers to the mass transport (or diffusion) limitation. In order to ensure that electroactive species are delivered to the electrode interface at a rate matching their consumption, it's necessary to overcome mass transport resistances by building a well designed water and gas flow.

This term is governed by the Nernst equation 2.25 which states that as the concentration of the product species at the reaction interface increases, the overpotential caused by mass transport limitation also increases

$$\eta_{diff} = \frac{RT}{nF} \log\left(\frac{C}{C_0}\right) \tag{2.25}$$

Usually the mass transport phenomena occur at very high current densities so many authors neglect to take these into account.

Kinetic overpotentials of HER and OER

As the mechanisms of the OER in both acidic and basic media involve multiple steps, Man et al. [70] proposed an expression for calculating the theoretical overpotential at $U = 0$ versus the SHE by examining the thermodynamics of the process. However, it was observed that this theoretical value significantly differed from experimental values. This disparity underscores the fact that when studying the thermodynamics of overpotential, kinetic constraints are not taken into consideration.

For this reason, overpotential at a fixed current density, typically 10 mA/cm_2, is considered a quantitative parameter to evaluate an electrocatalyst for both the HER and OER. This approach accounts for the kinetic aspects of the reactions and provides a more accurate assessment of electrocatalyst performance.

2.7.2 Tafel slope and exchange current density

The Tafel slope and exchange current density are two kinetic parameters that are derived from Tafel plots that help to characterize the efficiency and performance of electrocatalytic processes. These parameters are obtained by graphing the polarization curves as $\log j$ (current densities) versus the overpotential η. The Tafel equations for the anodic and cathodic polarization curves reported in 2.27 arise from the high overpotential approximation of the mentioned Butler-Volmer equation 2.17

$$\log j = \log j_0 + \frac{\beta n F}{RT}\eta \tag{2.26}$$

$$\log j = \log j_0 - \frac{(1-\beta) n F}{RT}\eta \tag{2.27}$$

Both equations are in the linear form, therefore the obtained slope are:

$$\frac{\mathrm{d}\log j}{\mathrm{d}\eta} = \frac{2.303RT}{\beta n F} \tag{2.28}$$

$$\frac{\mathrm{d}\log j}{\mathrm{d}\eta} = -\frac{2.303RT}{(1-\beta) n F} \tag{2.29}$$

As introduced in section 2.5.2 , the mechanism by which HER proceed is studied by the value of the Tafel slope and is based on the coverage of the H_{ads}.

When the H_{ads} surface coverage is low hence the distance between adjacent sites exceeds the Van der Waals radius, H_{ads} react with a proton and electron simultaneously leading to Heyrovsky reaction [57]. Indeed, in the case of the Tafel mechanism, it is essential that the separation between the surface active sites does not exceed the Van der Waals radius of the two adsorbed hydrogen atoms.

A smaller distance between these sites increases the probability of chemical desorption, that's why the Tafel mechanism is less liked.

The exchange current density, on the other hand, is determined by extrapolating a linear fit to a point where the current density (on a logarithmic scale) intersects with the equilibrium potential of the electrocatalytic process. A higher exchange current density indicates a more effective electrocatalyst. It provides insights into the inherent rate of reaction transfer between the electrode and electrolyte under equilibrium conditions and depends on the temperature, the electrocatalyst material and its load [64] and the analyte in solution.

When the exchange current density is high, electron transfer across the catalytic interface is efficient, requiring very little activation energy. Indeed, since the Tafel slope reflects the rapidity of the reaction kinetics, for an electrocatalyst to be considered ideal for water splitting, it should exhibit: low overpotential, a small Tafel slope value, and a substantial exchange current density.

2.7.3 Faradaic Efficiency

The Faradaic Efficiency (FE) in an electrolytic process provides a clear and objective assessment of the effectiveness of that process in converting electrical energy into desired chemical energy. It is defined as the ratio between the actual and the theoretical maximum quantity of hydrogen produced by the electrolyser at a given operating condition.

$$\eta_F = \frac{V_{\mathrm{H_2,real}}}{V_{\mathrm{H_2,th}}} \tag{2.30}$$

The theoretical quantity of hydrogen can be calculated as follow:

$$V_{\mathrm{H_2}} = V_M \left(\frac{10^3 ml}{I}\right)\left(\frac{t(60s)}{min}\right)\left(\frac{I}{2F}\right) \tag{2.31}$$

where n_c represents the number of cells in the stack, V_M the ideal gas expression ($V_M = R(273+T)/P$) and the ideal gas constant (0.0821 $atm/molK$), pressure (atm), temperature are denoted R, P, t respectively.

It's important to emphasize that most Faradaic losses in the electrochemical process are attributed to the formation of byproducts or heat loss. An electrocatalyst can be considered suitable for commercialization in water splitting applications if its FE is at least 90 %. The Faradaic Efficiency for PEM technology has the highest values due to the presence of the membrane separating the two gases produced, bordering on values close to 100 %.

2.8 Efficiency

On the basis of the simple theoretical description provided and the explanation of the effects that most influence the operation of the cell, from a purely constructional point of view, it is possible to write down some process efficiencies.

Thermal/Cell Efficiency

It is nothing more than the ratio between the variation in the enthalpy of reaction $\Delta H^0{}_{\mathrm{r,298\ K}}$, which is the calorific value on a molar basis of hydrogen (that essentially signifies the energy extracted during the process), and the energy injected into the cell, given by the number of electrons involved in the reaction multiplied by the Faraday's constant and the real time voltage applied to the cell.

$$\eta_{th} = \frac{\Delta H^0{}_{\mathrm{r,298\ K}}}{nFU} \tag{2.32}$$

The resulting energy efficiency can be expressed by the equation 2.33.

$$\eta_e = \frac{U_{tn}}{U} \tag{2.33}$$

Overall Efficiency

In accordance with part of the objectives of the study, it is possible to extend the analysis to the efficiency of the entire electrolysis process (also considering the consumption of auxiliaries) instead of limiting it to the individual cell. By considering the electrolyser

as a kind of 'black box' into which we put deionised water and electricity, and only obtain hydrogen as a useful product as an output, we can express this relationship:

$$\eta = \frac{\dot{q}_{H_2 \cdot HHV}}{P_{el}} \qquad \eta = \frac{\dot{q}_{H_2 \cdot LHV}}{P_{el}}$$

where HHV and LHV are reported in the Hydrogen Fundamentals (Chapter 2.1) and $\dot{q}_{H_2}$ is referred to the hydrogen mass flow rate.

2.9 Electrolysis Technologies

The different water electrolysis technologies can be categorized based on the type of electrolyte, separators, working temperatures and pressures employed.

With regards to the work of Tang et al. [71], Chatenet et al. [48], etc... to enhance the comprehension, an overview of the main types of water electrolysis systems (summarized in Figure 2.7 and Table 2.3) is provided.

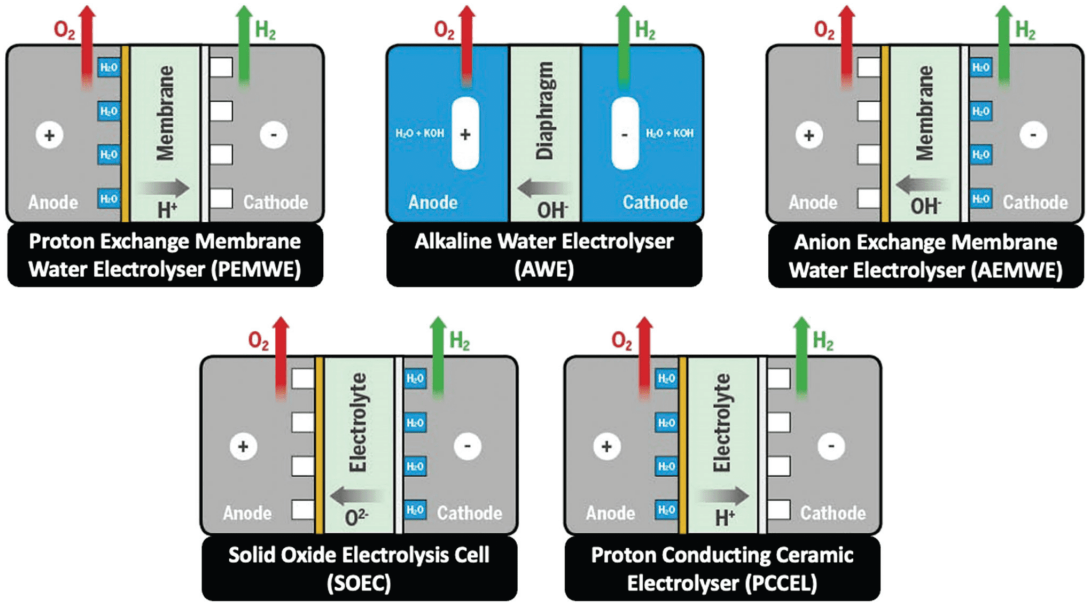

Figure 2.7: Different Electrolyzers Tecnologies. Image reported from [48]

2.9.1 Alkaline Water Electrolyzer

Standard AWE

Alkaline water electrolysis is the most mature hydrogen production technology via electrochemical water splitting, up to the megawatt range for commercial level in worldwide. The fundamental design of an alkaline water electrolyzer is characterized by its simplicity.

	AWE	**PEMWE**	**AEMWE**	**SOEC**
Operating temperature	$70-90°C$	$50-80°C$	$40-60°C$	$700-850°C$
Operating pressure	$1-30$ bar	<70 bar	<35 bar	1 bar
Electrolyte	KOH $5-7mol/l$	PFSA membranes	DVB polymer support with KOH or NaHCO3 $1mol/l$	Yttria-stabilised zirconia
Separator	ZrO_2 stabilised with PPS mesh	Solid electrolyte	Solid electrolyte	Solid electrolyte
Electrode/catalyst (oxygen side)	Ni coated perforated stainless steel	IrO_2	High surface area Ni or NiFeCo alloys	Perovskite-type (LSCF, LSM)
Electrode/catalyst (hydrogen side)	Ni coated perforated stainless steel	Pt nanoparticles on carbon black	High surface area Ni	Ni/YSZ
PTL anode	Nickel mesh	Pt coated sintered porous Ti	Ni foam	Coarse Ni-mesh or foam
PTL cathode	Nickel mesh	Sintered porous Ti or carbon cloth	Ni foam or carbon cloth	-
Bipolar plate anode	Ni-coated stainless steel	Pt-coated titanium	Ni-coated stainless steel	-
BP cathode	Ni-coated stainless steel	Au-coated Ti	Ni-coated stainless steel	Co-coated stainless steel

Table 2.3: Summary table of the different technologies, reported from IRENA [44]

It comprises two metallic electrodes separated by a porous separator that is soaked in an alkaline electrolyte solution, commonly KOH or NaOH. In these cells, the metallic electrodes are immersed in an aqueous electrolyte solution, typically containing $25-40$ $wt\%$ of KOH or NaOH. To ensure optimal electrical conductivity, the operating temperature is maintained within the range of $70-90$ $°C$. It's worth noting that KOH exhibits a specific conductivity of 0.184 S/cm at $25°C$. The reduction of water takes place at the cathode:

$$2H_2O + 2e^- = H_2 + 2OH^- \quad (U_C^0 = -0.828\text{V vs. SHE}) \tag{2.34}$$

while the hydroxyl ion oxidation occurs at the anode:

$$2OH^- = 1/2O_2 + H_2O + 2e^- \quad (U_A^0 = 0.401\text{V vs. SHE}) \tag{2.35}$$

The hydroxyl ion OH^- serves as the primary ionic charge carrier in this system, facilitated by the presence of KOH and water, which permeate through the porous structure of the diaphragm to enable the electrochemical reaction. This arrangement allows for the mixing of the produced hydrogen and oxygen, which dissolve into the electrolyte. Such mixing limits the operating range at low power and the ability to operate at higher pressure levels additionally has adverse consequences in terms of safety of operation and in gas purity [72].

To address this issue, thicker diaphragms ($0.2-0.25$ $[mm]$) are often employed. However, this thicker diaphragm design increases resistance and reduces overall efficiencies. Some manufacturers also include spacers between the electrodes and diaphragms to further prevent gas intermixing. These thicker diaphragms, along with added spacers, result in

higher ohmic resistances across the two electrodes, leading to a significant reduction in current density at a given voltage.

Two different connection configurations are used for industrial applications (Figure 2.8): the individual cells can be connected in parallel (monopolar assembly), or in series (bipolar assembly). In the former case, all anodes (or cathodes) are interconnected in parallel, typically through copper conduction bars. This configuration is employed to reduce Ohmic losses and ensure uniform current distribution. In the second scenario, the connection is achieved through endplates located at the two ends of the assembly, where the cathode of one unit cell is electrically connected to the anode of its neighboring unit cell. Both monopolar and bipolar configurations have their respective advantages and disadvantages. However, the bipolar configuration is generally more energy-efficient.

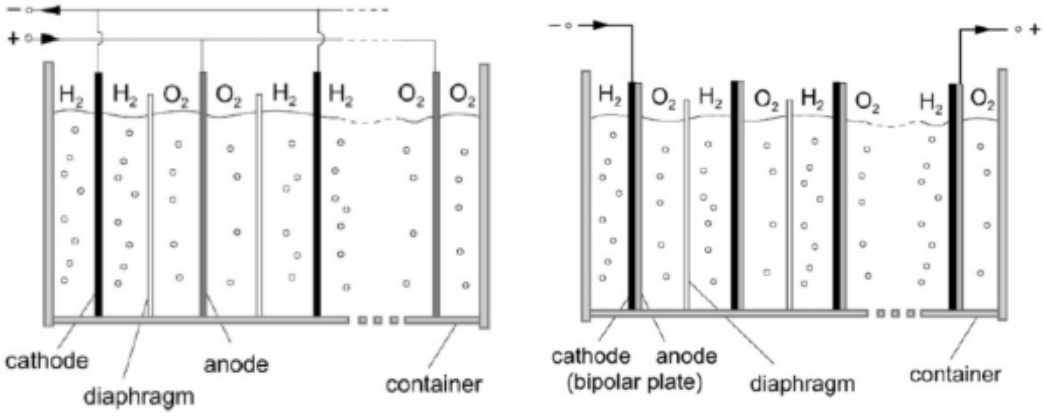

Figure 2.8: Electrolyzer connection configurations

In practical applications, AWE require several hours to achieve a steady state in terms of electrolyte flow, temperature and current density [73]. Some negative aspects are also known, such as limited current densities (below 400 mA/cm2), low operating pressure and poor energy efficiency. This characteristic makes it challenging to operate in a transient regime, which can be inconvenient when coupling them with renewable energy sources.

Anion Exchange Membrane Water Electrolyzer (AEMWE)

Alkaline Anion Exchange Membrane (AAEM) electrolysis represents a promising avenue in the field of hydrogen production. It brings together the favorable attributes of two distinct electrolysis technologies: the milder operating conditions of alkaline electrolysers and the efficiency of Proton Exchange Membrane (PEM) electrolysis. This hybrid approach unlocks several advantages, including the use of cost-effective non-noble catalysts (thanks to the alkaline environment) and the ability to operate under differential pressure as PEM systems do [74].

However, the possibility of exploiting the full potential of AAEM is still unrealistic. AAEM membranes face chemical and mechanical stability problems, and achieving the desired performance levels remains an obstacle due to factors such as AAEM's limited

conductivity, sub-optimal electrode design and slow catalyst kinetics. A noteworthy drawback is the inherently slower conductivity of hydroxide ions (OH^-) compared to that of protons (H^+) in PEM systems, requiring the development of thinner membranes or higher charge densities.

2.9.2 Proton Exchange Membrane Water Electrolyzers

Introduced for the first time in 1960s by General Electric, PEMWE was the first water electrolyzer based on a solid polymer electrolyte concept. This technology bears resemblance to fuel cell technology, where a solid polysulfonated membrane, such as Nafion® from DuPont, plays a crucial role in ensuring high proton conductivity, minimal gas crossover, a streamlined system design, and the capability for high-pressure operation.

The membrane and its thickness (20-300 μm) is in part the reason for many of the advantages of the solid polymer electrolyte: i) A significantly higher current density load, exceeding 2 A/cm^2, is feasible [75]. This capability serves to reduce operational costs, which in turn can lower the overall cost of electrolysis. However, it's essential to note that ohmic losses impose limitations on achieving these high current densities. Yet, because of a thin membrane, an excellent proton conductivity, typically in the range of 0.1-0.02 S/cm, could be feasible. ii) The low gas crossover rate ensures the production of ultrapure hydrogen, making it an economically viable choice. This advantage arises from the fast response of proton transport across the membrane to changes in power input without any delay related to inertia as could happen for liquid electrolytes [76]. iii) PEM electrolysis stands out by covering practically the entire range of nominal power density, spanning from 10 % to 100 %. iv) A compact system design with robust structural properties that can withstand high operational pressures (potentially reaching up to 70 bar in some commercial models) is also achieved by the low operational temperature range (50–80 $°C$). High-pressure operation has its advantages such as the delivery of hydrogen at a high pressure, which reduces the energy required for further compression and storage. Additionally, it minimizes the volume of the gaseous phase at the electrodes, significantly improving the removal of produced gas following Fick's law. In a differential pressure configuration, only the cathode side is under pressure, eliminating the handling hazards associated with pressurized oxygen and the risk of Ti-ignition in the oxygen environments. The listed advantages simultaneously combine to ensure high efficiency and a reduced environmental footprint.

However, the biggest drawbacks associated with PEM electrolysis is related to the corrosive acidic environment created by the proton exchange membrane that necessitates the use of specialized materials. These materials must not only withstand the harshly corrosive low pH conditions but also endure high applied overvoltage, especially at high current densities. Corrosion resistance is crucial not only for the catalysts employed but also for current collectors and separator plates. This leads to the use of scarce and extremely expensive materials, including noble catalysts like PGM (i.e. Pt, Ir, and Ru), Ti-based current collectors and separator plates. Furthermore, as far as pressure is concerned, it is

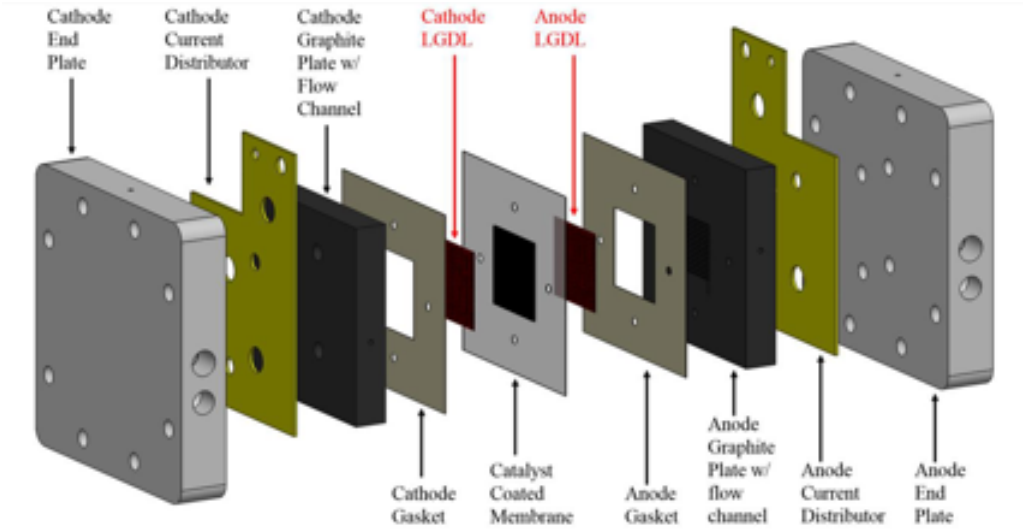

Figure 2.9: Exploded view of a PEM cell

true that it is possible to operate up to 70 *bar*, but at the same time crossover phenomena increase dramatically [26], causing premature ageing of the membrane and the resulting safety problems, as well as the reduced hydrogen quality, etc.

During the operation of a PEM cell, deionised water is pumped to the anode where it is spilt into oxygen, protons H^+ and electrons e^-. The protons travel through the Membrane-Electrode Assembly (MEA) and the electrons through the external power circuit (which provides the driving force) in order to reach the cathode side. At the cathode side protons and electrons recombine to produce hydrogen, according to the following reaction path:

$$H_2O = 1/2O_2 + 2e^- + 2H^+ \quad (U_A^0 = +1.229\text{V vs. SHE}) \tag{2.36}$$

$$2H^+ + 2e^- = H_2 \quad (U_C^0 = 0.000\text{V vs. SHE}) \tag{2.37}$$

As illustrated in figure 2.9, the components of a PEM water electrolysis cell are: the End Plates, the Current Collectors with Gas Diffusion Layers (GDL), the Membrane Electrode Essemblies (MEAs), and the Separator Plates.

Besides the end plates, which are constructively the simplest, not subject to particular corrosion, or at least largely negligible compared to other components, a brief description of the other components is given below.

Separator plates

The Separator plates account for a significant portion of the overall cell cost and they play a direct role in determining the required cell voltage. It must provide structure to the cell, insulation between the reactant gasses and a conductive path for the heat and the

electrons. Presently, are composed of materials such as titanium, precious metal coated stainless steel and graphite. However, these materials are associated with high costs and come with various operational limitations.

Indeed, Titanium is a commonly chosen material due to its excellent strength, low initial resistivity, high initial thermal conductivity and low permeability, however, it is susceptible to corrosion on the anode side, leading to the formation of an inert oxide layer that adversely affects the performance. To mitigate these issues and protect titanium plates, the application of precious metal coatings and alloys have proven effective in significantly reducing the corrosion rate.

Coatings can greatly improve the life of the components, however, creating and applying a coating that meets the demands of this environment is not easy, a low imperfection density is vitally important as once the base metal is exposed, corrosion will cause the coating to flake off, increasing the ohmic resistance and therefore the corrosion [77]. Nevertheless, this additional process incurs costs related to the precious coating materials and the already expensive base titanium. Consequently, the quest for cost-effective separator plates is still a challenge.

Graphite has been used frequently because its conductivity but its low mechanical strength, high corrosion rates and difficulty of manufacture has made it an increasingly less preferred choice.

In this regard, the need to reduce costs is paramount, both in the materials used and the complexity of the processing to achieve the desired surface structure. Indeed, this must facilitate the movement of water, promote its uniform distribution over the catalyst material, and promote the extraction of produced gases, as documented in various studies [78]. Among the various designs explored, the best performance, in the form of increased electrolytic activity, has been achieved by exploiting the straight parallel field design.

Membrane Electrode Assemblies

The Membrane Electrode Assemblies (MEA) are consisting of a membrane, a ionomer solution and anode, cathode electrocatalysts.

The most commonly used membranes are the Perfluorosulfonic acid polymer membranes such as Nafion®, Fumapem®, Flemion®, and Aciplex®, however, Nafion® membranes are the most commonly used because capable of operating at higher current densities (up to 2 A/cm^2) and temperatures, showing high durability, high oxidative stability, high proton conductivity, and good mechanical stability [75].

Most of the MEA are built by using the Catalyst Coated Membrane (CCM) method: the catalysts are directly applied on both the surfaces of the ion-conducting membrane to achieve high surface contact. Porous current collectors are then pressed against these CCMs and the adjacent electrolysis cells being stacked together and separated by the metallic bipolar plates [79].

In addition, a ionomer solution with ionic transport properties in the catalytic layers

is commonly used for two main reasons: the former is promoting the proton transport from the electrode layers to the membrane, thus increasing the cell efficiency by decreasing the ohmic losess. Further the ionomer solution act as a binder, making the structure dimensionally stable and consequently enhancing the durability of the electrodes [80].

Current Collectors

Current Collectors play a pivotal role in the functioning and the efficiency of PEMWE systems. A porous Titanium plate (prepared through thermal sintering of spherically shaped Titanium powder), enclosed by bipolar plates and sealed with gaskets, serve a dual role as both Current Collectors and GDL on both sides of the MEA.

Notably, current collectors must possess a combination of characteristics to meet the demanding conditions of PEM water electrolysis. They must exhibit corrosion resistance given the harsh acidic environment and the presence of oxygen. In addition, it is crucial to maintain good electrical conductivity over time while ensuring efficient gas expulsion and effective water delivery to the catalytic sites, especially under high current density conditions where mass transport becomes the limiting factor.

Balancing porosity in current collectors is critical; while large porosity facilitates gas removal, it can hinder electron transport and reduce efficiency. Conversely, excessive porosity obstructs gas expulsion and increases mass transport resistance [81]. Furthermore, achieving a homogeneous current distribution at the electrode-current collector layer surface is imperative to avoid the formation of hot spots that could potentially damage the membrane or create surface defects.

2.9.3 Solid Oxide Water Electrolyzers

In SOWE oxide-ion conducting ceramics (that conventionally uses the O_2^- conductors) are used both as the solid electrolyte and the cell separator. The electrolyzer operates at high pressure and high temperatures $800 - 1000°C$ and utilizes the water in the form of steam, therefore, the solid electrolyte used are generally zirconia that has been stabilised with yttrium and scandium oxides (YSZ) or manganite-coated stabilised zirconia.

During the process water vapour is reduced at the cathode and the resulting oxygen ions migrate to the anode, where O_2 evolves as shown by the reaction pattern below:

$$H_2O_g + 2e^- = H_2 + O^{2-} \quad (cathode) \tag{2.38}$$

$$O^{2-} = O_2 + 4e^- \quad (anode) \tag{2.39}$$

Oxide ions are transported from the cathode to the anode through the solid electrolyte via ionic diffusion process, facilitated by the use of ultra-thin ceramic membranes ($\sim 30-150$ μm) to minimize ohmic losses. The steam cathode is typically made of porous nickel,

while the air anode typically consists of porous perovskite materials, blended with various catalysts.

SOEC technologies have been motivated by the potential to operate at high current densities (3.6 A/cm^2 at 1.48 V and 950°C), achieving remarkable efficiency levels. Furthermore, the electrochemical processes, due to the elevated operating temperatures, are reversible. This feature allows a single SOEC unit to function as both a fuel cell and an electrolysis cell.

Chapter 3

Experimental Methods

A home-made test bench has been constructed for carrying out the experimental test and its components are listed below. The system was designed to be flexible and versatile so that it can be used to perform the tests under consideration and for future tests in a wide range of conditions.

The scheme that shows the position of each component is shown in Figure 3.1, while Figure 3.2 shows the concrete installation.

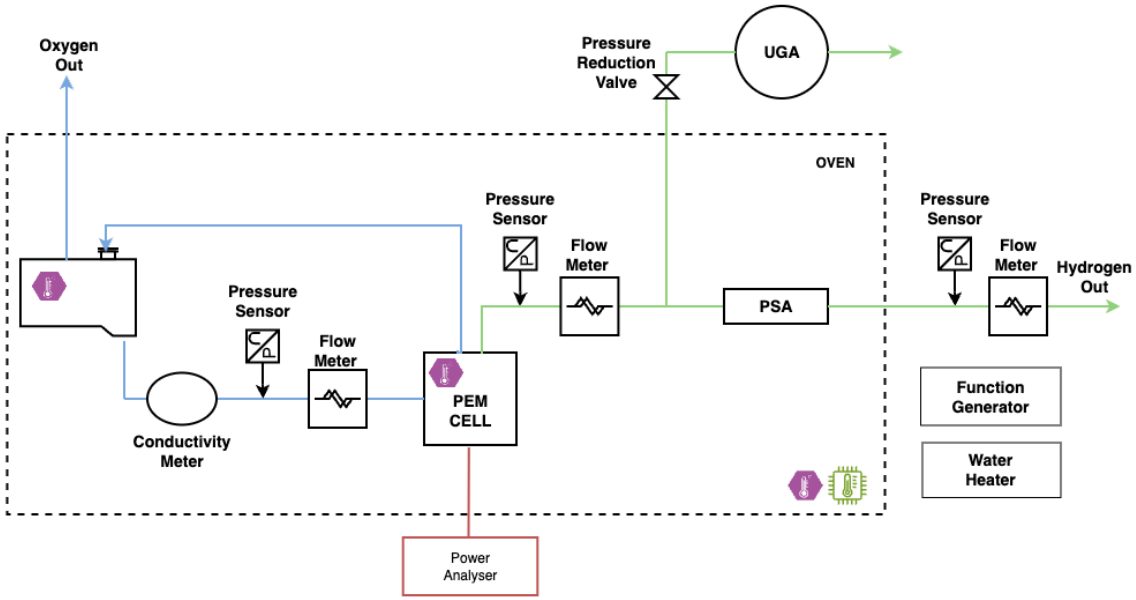

Figure 3.1: Plant scheme

- **LNI - HG RACK 2U PRO 350**: laboratory PEM electrolyzer capable of generating up to 350 cc/min of hydrogen at a pressure of up to 16 bar with a built-in PSA drying system. In addition to this, an **LNI hydrogen detection sensor** was also included. This sensor was fitted within the oven and, in case of a plant failure, it would promptly halt production, leading to the immediate release of all the hydrogen inside the pipe.

- A **Conductivity Sensor UPW 3/4NPT 0.1C Ti 2** and its transmitter **M800 Process 2-CH** by Mettler Toledo was used to record the change in conductivity of ultrapure water during the test phases and enable interface with the data acquisition system built using LabVIEW. The sensor was accurately fixed on the top lid of the water tank within the electrolyzer's own water loop.

- Three different **Kistler - Pressure Sensors**, two type **4045A50** and one type **4043A10**, each interfaced to its own transmitter were respectively positioned in the internal and external hydrogen circuit and in the water supply loop;

- A **Mini Cory Flow M14 - Coriolis Mass Flow Meter** by Bronkhorst was included in the water supply loop, specifically positioned between the water pump and the cell inlet. This data has never really been exploited, except to validate the minimum flow required for the conductivity meter;

- Two **EL Flow F111B - Thermal Mass Flow Meter** by Bronkhorst, positioned respectively at the output of the PEM cell and at the hydrogen output of the electrolyzer;

- Two **EL Flow Prestidge FG-210CV** were positioned before and after a **Pressure Reduction Valve** to understand the real consumption of the Universal Gas Analyzer hence the spillage rate from the main line.

- Three **Type K - Temperature Sensor** were positioned respectively on the Anode and the Cathode end plates and the last inside the internal water tank;

- A Standford Research System - SRS **UGA Series - Mass Spectrometer** was placed next to the oven and connected directly to the cell using the shortest possible route for the pipe;

- A **Precision Power Analyser LMG 640** by Zes ZIMMER with associated current and voltage sensors was used to record the consumption of the cell and of the entire system.

The listed components, most of them fitted inside the Dynamic Climate Chamber **BINDER MK 240 E3.1**, were used for each test. Only for determining the cell's characteristic, it was necessary to implement two additional tools: a programmable phase generator (ET System Electronic GmbH - LAB/HP 1020) which enabled the execution of the step test, and a water heating system (Lauda - LOOP L100) used to bring the cell to the desired temperature of $80°C$.

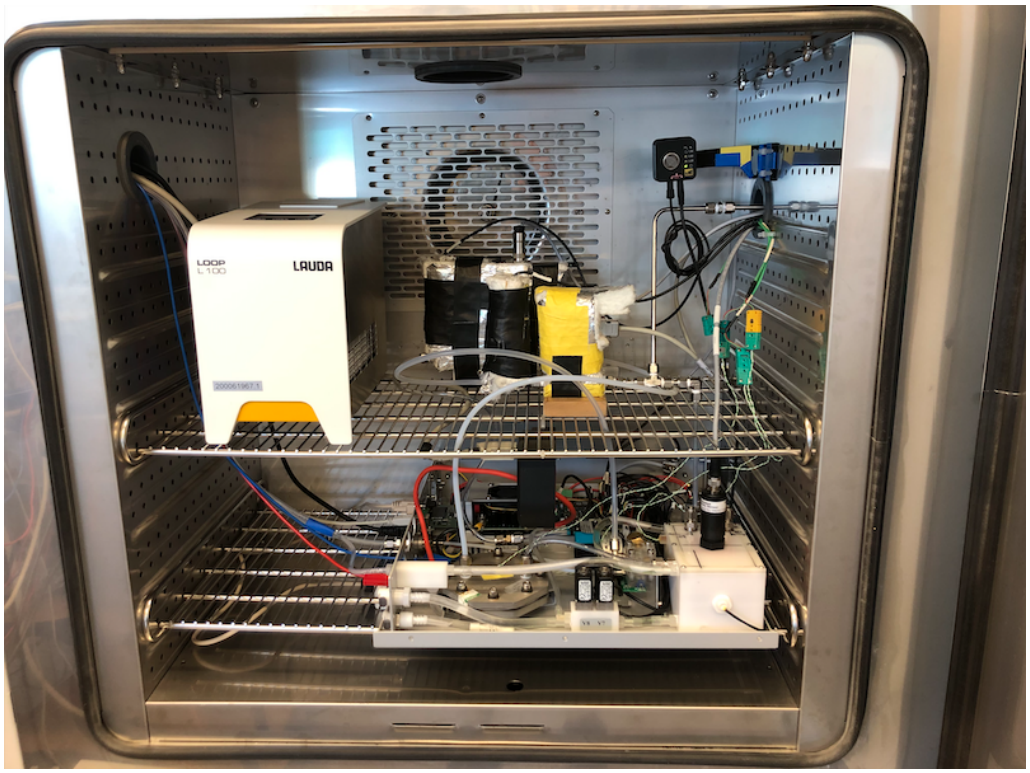

(a) External Temperature control method

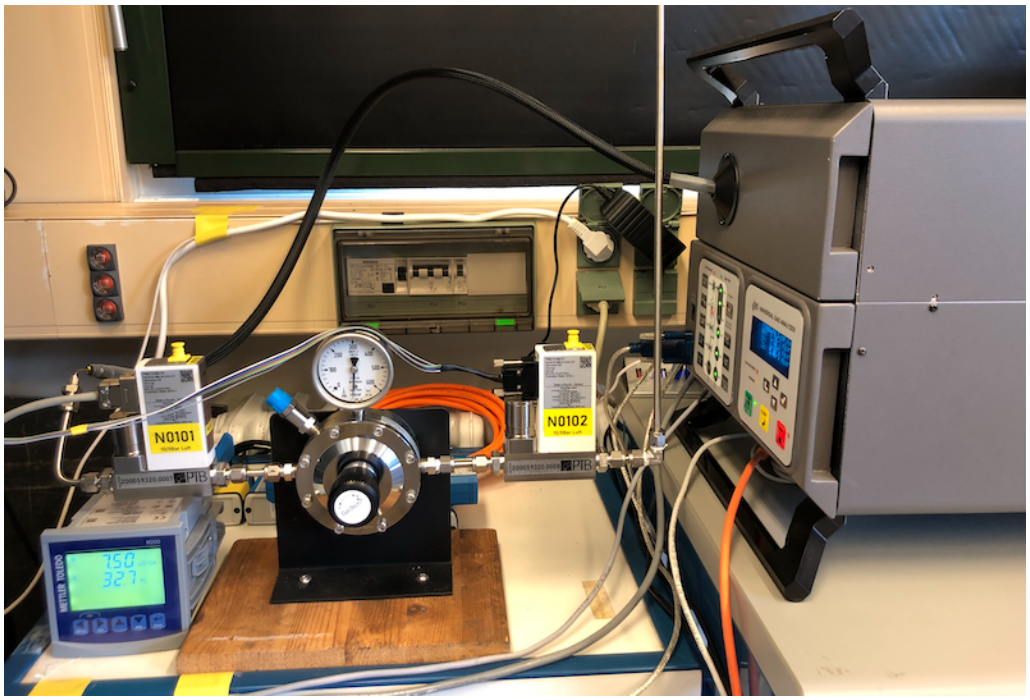

(b) Gas Analysis

Figure 3.2: Laboratory Setup

Chapter 4

Results and Discussion

The relevance of operating temperature as a driving factor for the cell component consumption was introduced and adequately illustrated. Indeed, to better understand, a theoretical background on the phenomena governing electrolysis was provided. In particular: the characteristic reaction patterns, the equations modelling and determining the occurrence of the different scenarios, and the process evaluation parameters were provided. This makes it possible to adequately understand the investigated results with the experimental system set up.

4.1 Experimental Protocol

According to the scientific literature, as of today, there is no specific test used to investigate certain or all the characteristics of an electrolyzer. Referring to the works of Andrej Zvonimir Tomic et al. [16] and Christoph Rakousky et al. [6, 82], which deal with degradation and testing procedures for PEM electrolyzers, the majority of tests conducted tend to extend over very long time spans (over 1000 hours) and are primarily used to estimate the useful life of a cell, analyzing the factors that have led to its failure. However, these tests typically involve input current in various forms: constant, variable, or a combination of both.

Some of the most important considerations that led to the development of the test under examination are as follows: i) Characteristic analysis times are too long. ii) In accordance with the literature, it has been concluded that it's not just the variability of input power that determines high wear phenomena, but rather it's the temperature and operating pressure that dominate. Therefore, it is necessary to focus attention on these parameters.

In this study, temperature is taken as the primary parameter.

Most of the tests are conducted at $80°C$ without considering that the actual operation of the electrolyzer is characterized by significant fluctuations between ambient temperature and operating temperature, not only caused by a change in input power. Frensch et al. [83] reported that a temperature change from 60 to $90°C$ results in increased efficiency

but also accelerates degradation processes. A maximum temperature of $80°C$ is therefore suggested as a compromise between consumption and performance. Siracusano et al. [31] investigated the effect of varying the operating temperature between 25 and $80°C$ during a simultaneous variation of power between 1 and 3 A/cm^2. However, the test does not consider high current density and low-temperature operations simultaneously, as seen in real-world scenarios. iii) The quality of the produced hydrogen, although the highest, has never been investigated in line, except for alkaline electrolyzers [13]. It is, therefore, interesting to analyze whether a variation in operating temperature significantly affects the quality of the produced hydrogen. iv) Favorable start-up behaviors of the electrolyzer have been recently and extensively addressed by [84], but tests for different initial external temperature conditions have not been conducted.

4.1.1 Experimental Procedure

The devised protocol consists of five tests carried out in an identical manner, except for the initial external temperature conditions, which are set at 1, 5, 15, 25 and $35°C$, represented in Figure 4.1a respectively. Going below $1°C$ would have been ideal, but it would have required preheating of both water and the cell to prevent freezing phenomena.

Anyhow, even in an uncontrolled environment as long as it's enclosed, for external temperatures dropping below $0°C$, the internal temperatures, due to the dissipation of the electrolyzer itself and the enclosures protecting the structure, should not deviate significantly from the assumed minimums.

The measurement instruments inside the controlled-temperature environment as well as all the pipelines were cleared of any condensation that may have accumulated when the machine was turned off, then they were brought to the desired operating temperature until reaching a pseudo-thermal equilibrium.

Upon reaching the desired conditions, the data acquisition system was initiated, with data acquisition carried out through LabVIEW and the Residual Gas Analyzer. After verifying the correct acquisition of each instrument, the electrolyzer was then started. Since there was no direct control over the input current value, but only indirect control based on the theoretical amount of hydrogen produced, the electrolyzer was consistently operated at 80% of its maximum production capacity. This translated to an almost constant specific-current input value of approximately 0.625 A/cm^2, as shown in Figure 4.1b. It is important to emphasise that in relation to the scientific literature, where such specific current is considered low, this does not apply to the above-mentioned cell, as the potential it takes on at this current density is extremely high.

The system was then brought to its operating internal pressure $\simeq 15$ bar (Figure 4.1c) in 'valve closed' mode to allow for rapid pressurization. Subsequently, the external valve was opened, and the hydrogen was released at a pressure of approximately 2 bar. It is important to emphasize that reaching this pressure is ideal especially for the Pressure Swing Adsorber (PSA), an auxiliary system that allows the adsorption of specific impurities

in the produced hydrogen, the necessity of which is also being evaluated. During this phase, the cell operated at a specific current lower than the nominal current $\simeq 0.473\ A/cm^2$. The purpose is presumed to be a gradual pressurization of each component to the operating pressure, avoiding steep gradients, and limiting the potential as suggested by [84].

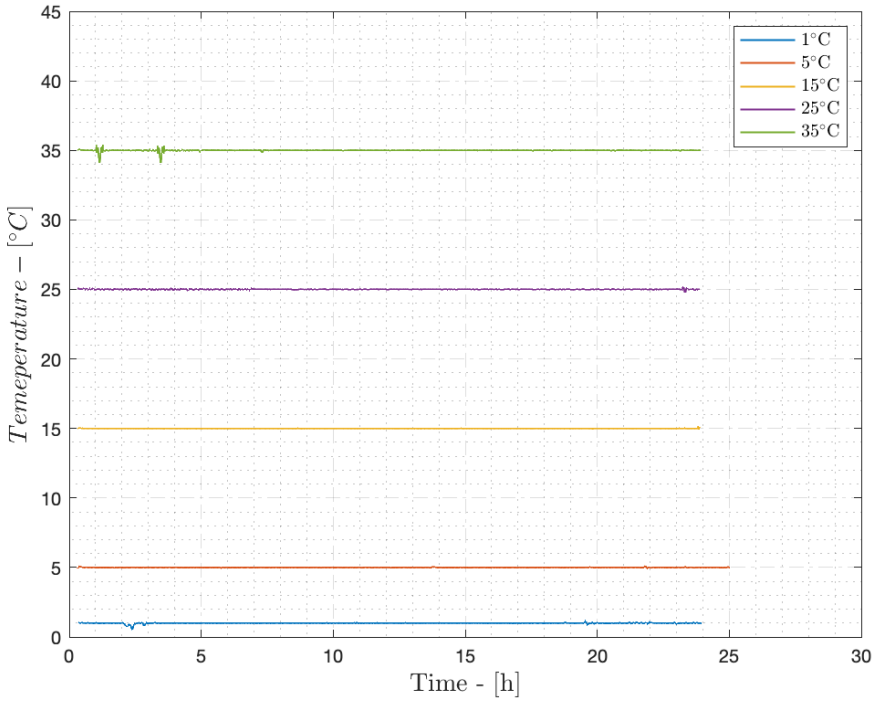

(a) Different External operating Temperatures

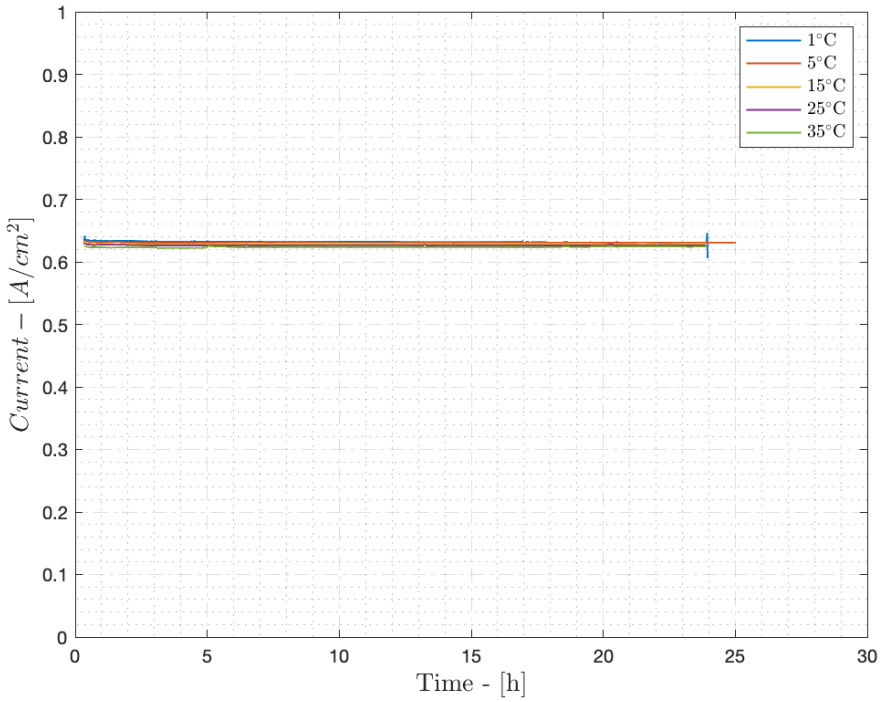

(b) Current values for each steady state test

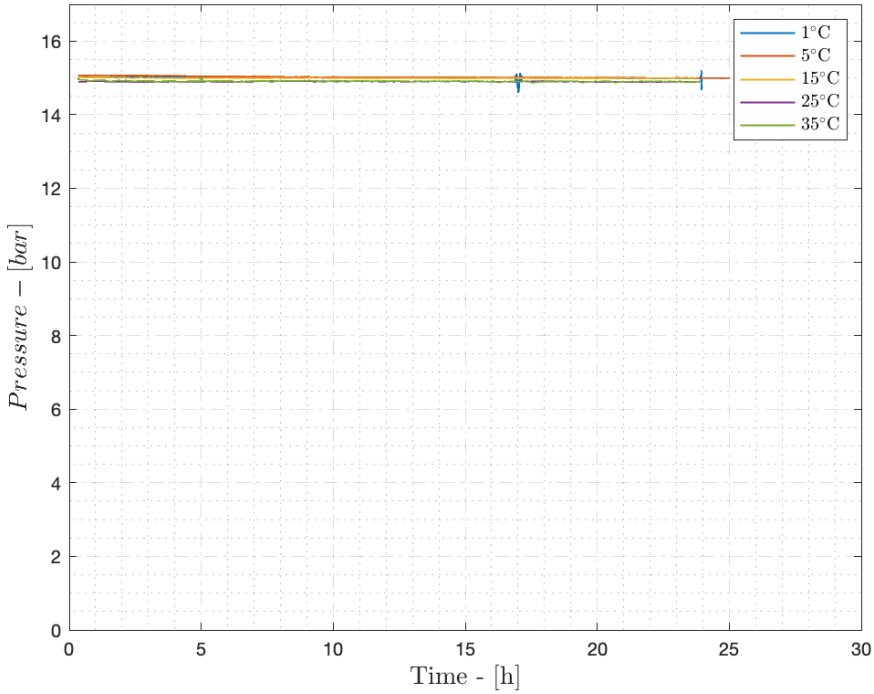

(c) Internal pressure values during steady state current

Figure 4.1: Test Procedure

Subsequently, each test was extended for the following 24 hours, roughly the minimum time required to analyze the effects that temperature could have on various aspects of the system's operation.

4.2 Cell Characterization

Before any test, the (I-V) polarization curve was carried by following the EU harmonised polarisation curve test method for low-temperature water electrolyzer [85]. The main objective of the polarisation curve measurement is to determine the change in the cell/stack voltage (and consequently in supplied power or power density) generated by the variation in the supplied current under steady-state conditions, and in particular at a constant cell/stack temperature and a constant hydrogen (and/or oxygen) pressure. The polarisation curve measurement was performed under galvanostatic control, at $80°C$ in agreement with most of the authors, by following the proposed method B (stepwise steady-state current sweep): consecutive defined current density steps, reported in the Appendix A.

The step test and the resulting polarization plot are reported as follow in Figure 4.2

As recommended by the testing protocol, the measurement should be aborted when the cell voltage is 2 V or above (cutoff voltage), but since the used cell was certainly not built with the state-of-the-art materials, the operating potential was always close to 2 V even for minimal power input. For this reason, the test was extended until the end of the incremental steps, hence 2 A/cm^2.

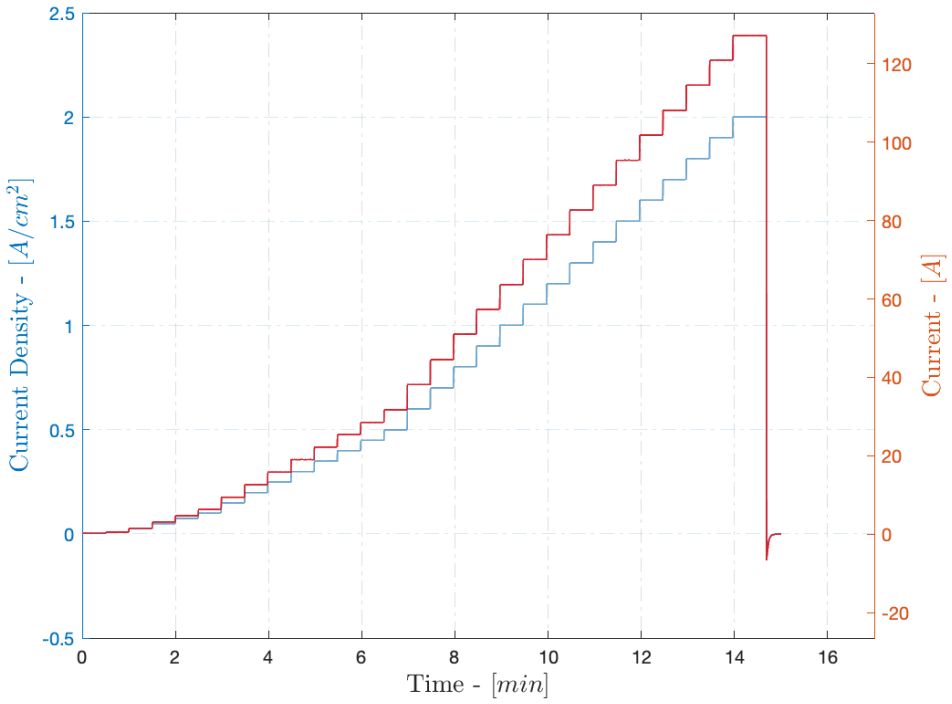

(a) Step Test performed according to [85]

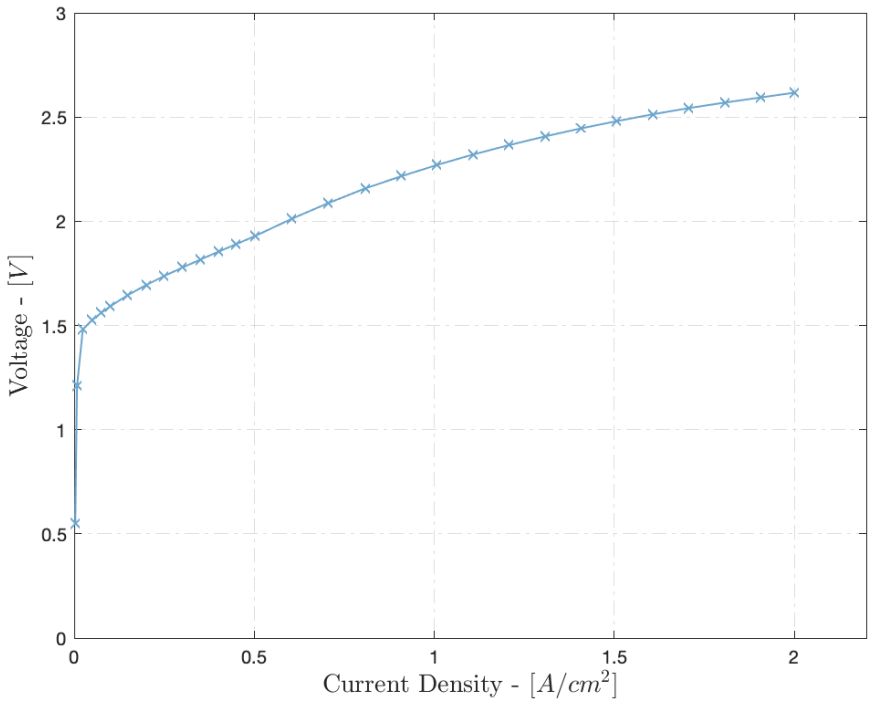

(b) Polarisation curve @ $80°C$

Figure 4.2: Cell Performance

As can be seen from Figure 4.2b, the polarisation curve is entirely in accordance with what is reported in the literature in Figure 2.6. The cell also does not exhibit any mass transport phenomena in the analysed field.

4.3 Experimental Efficiency

The first objective of this work concerns the influence of external temperature on both the only cell efficiencies and the overall process. Its experimental determination, in addition to highlighting deviations from theory (which often assumes a constant operating temperature determined by the water supply), is an interesting result for assessing the operation of an extremely simplified system in which the operating temperature is not controlled, except for its maximum value.

It is clear that for big-sized electrolyzers, a cooling system is necessary as the operating temperature tends to increase. It is also true that so far, these electrolyzers have been used in continuous, and their operation with renewable sources may not even bring them up to temperature within days if there are no specific controls for rapid heating, as analyzed by [84], especially if the external temperature is considerably cold.

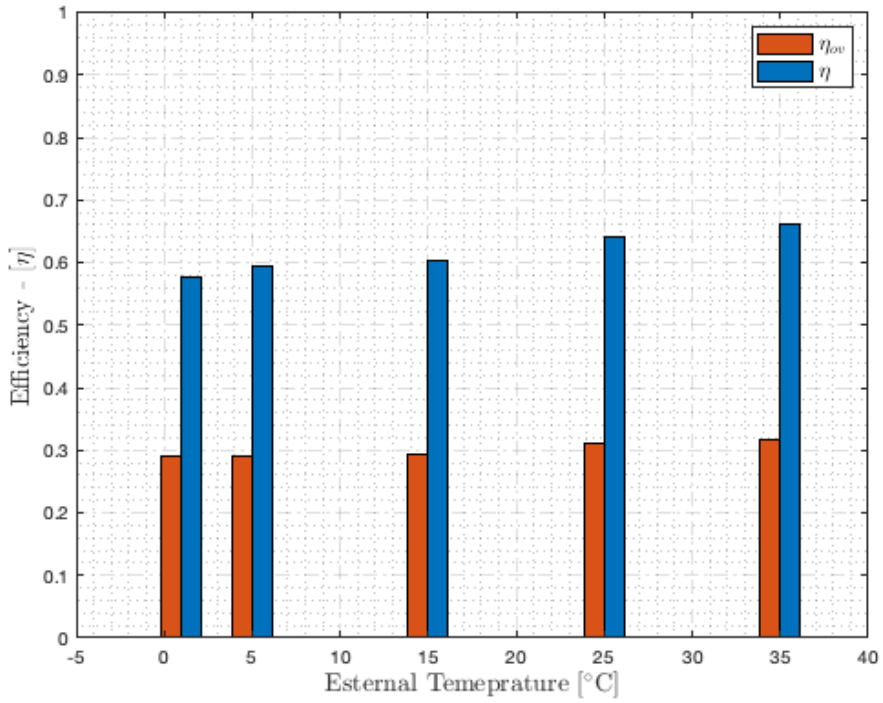

Figure 4.3: Efficiency values over different external temperatures

Figure 4.3 illustrates what has just been mentioned. The chart displays the average cell efficiencies (blue) and overall efficiencies (red) with reference to HHV, calculated according to equation 2.8.

From this graph, it becomes evident that temperature has a distinct influence on the two cases. The cell is indeed undoubtedly governed by external conditions, while the complete system experiences a less pronounced impact since the cell is a significant but not dominant part of consumption.

This is evident when analyzing the hydrogen production rate graph (Figure 4.4): the

input current (automatically controlled by the machine) is almost constant (Figure 4.1b), so the variations recorded in the volumetric flow measurement are due to the effects of hydrogen solubility in water, gas temperature and pressure conditions, as well as data acquisition, which is certainly not free of noise.

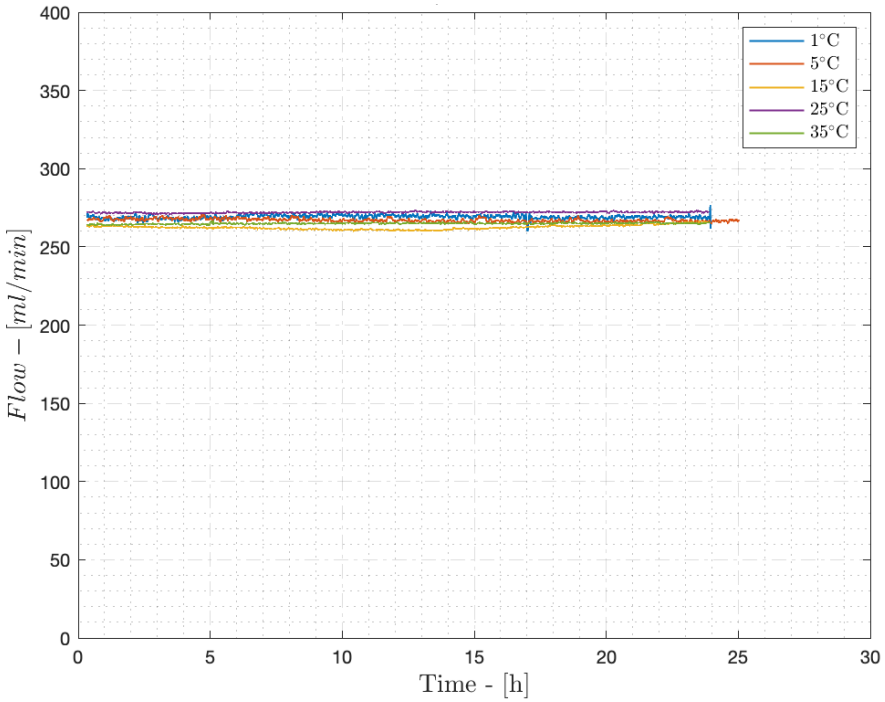

Figure 4.4: Hydrogen Internal Flow

The measurement instruments employed, the majority of which were initially calibrated for operation within ambient room temperature conditions, demonstrated acquisition behavior, as depicted in Figure 4.5, primarily attributed to two key factors.

The most impactful factor arises from the exposure to low temperatures, specifically at 1 and $5°C$, coinciding with the instruments' operation at the extreme boundaries of their designated operational range.

Conversely, the second factor, characterized by a persistent low-level noise, unequivocally emanates from the inherent characteristics of the analog acquisition system. It is noteworthy that the output from a substantial portion of these instruments indeed presented as a voltage potential spanning the range of 0 to 5 volts, which inherently yields a measurement exhibiting greater noise levels when compared to a current-based measurement.

However, the high sampling rate of the acquisition allowed for precise noise cleaning.

All the recorded data were then converted to the standard conditions (STP) using the correction factors provided directly by Bronkhorst.

Nevertheless, it is important to clarify that the observations drawn from this data (as well as the following ones) are all evaluative and should not be interpreted as definitive. The electrolyzer is, after all, a laboratory model, and the effects of a system operating at the MW power level could (even if only slightly) differ from what is presented here.

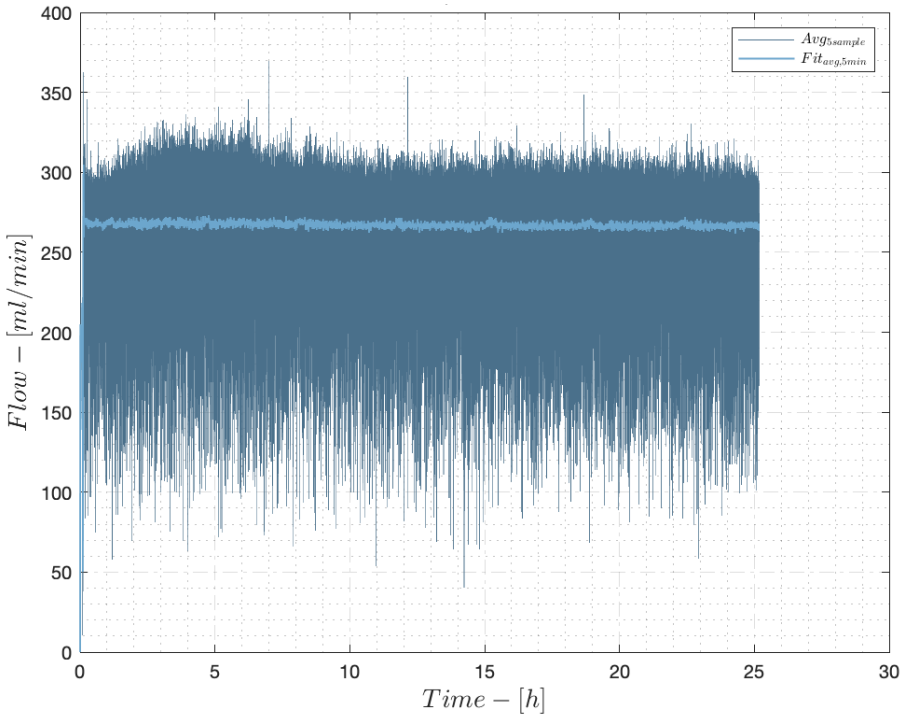

Figure 4.5: Hydrogen Internal Flow: worst-case scenario, raw and fitted data @ $5°C$

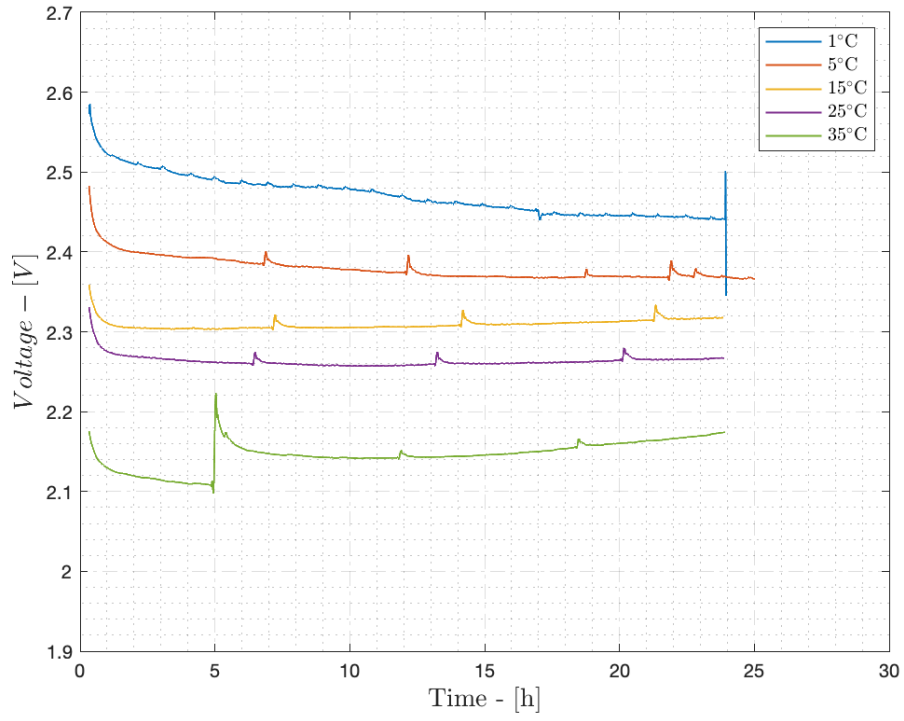

Figure 4.6: Evolution of the Cell Voltage for different External Temperatures

Because of the data acquisition, which is noisy under certain circumstances, and because of the inherent characteristics of the PEM technology, which, thanks to the membrane, allows optimal gas separation, the Faradaic Efficiency was not calculated.

Therefore, since hydrogen can still be considered an ideal gas under the pressure and temperature conditions in question, the variation in its density complies with the perfect gas law.

As a result, the mass flow rate produced remains almost constant in all the tests conducted, and consequently, the energy derived from it.

Despite the nearly constant mass production rate, energy consumption experiences a significant increase, primarily due to the rise in overpotentials as could be clearly seen in Figure 4.6. Consequently, cell efficiency decreases by approximately 10 % compared to the overall efficiency, which only shows a variation of $3 - 4$ %.

4.4 Impact of Temperature Variation on System Parameters

Referring to the figure 4.6, as well as observing the marked difference for different operating temperatures, a clear difference in the slopes of the curves can also be noticed. At low temperatures, i.e. at 1 and $5°C$, the slope of the recorded potential is consistently decreasing. At intermediate temperatures, such as 15 and $25°C$, the slope remains almost constant, while at $35°C$, the slope initially decreases and subsequently shows a constantly increasing trend.

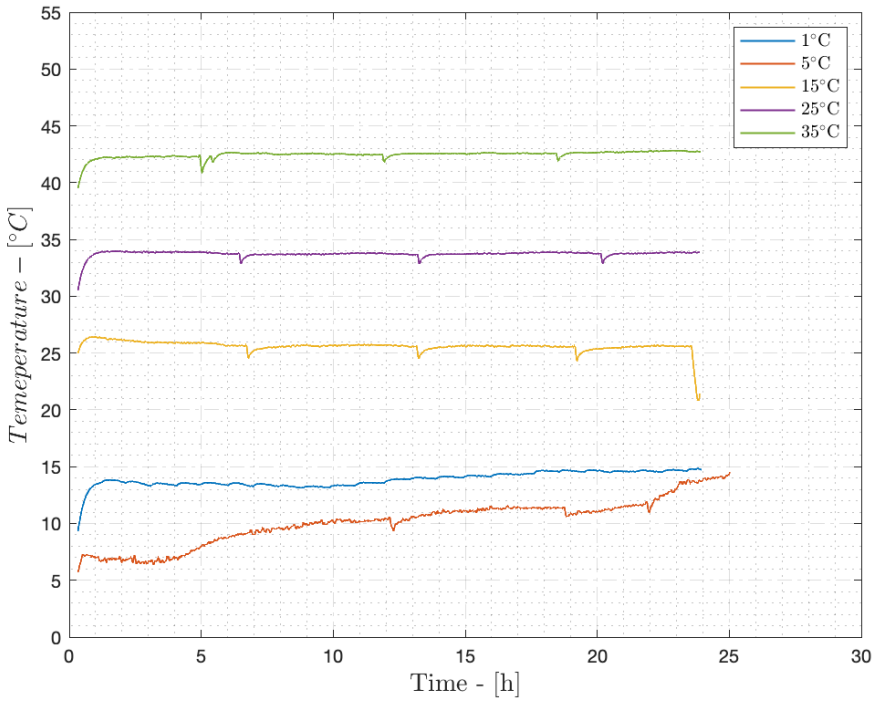

Figure 4.7: H_2O Equilibrium Temperature

To explain this phenomenon it is assumed that the factors influencing these differences are mainly two. The former is referred to the Reaction Kinetics. At low temperatures, reaction kinetics decrease dramatically, and the time required to reach a constant potential,

or equilibrium potential, increases. Even though the cell is in thermal equilibrium (as shown in Figure 4.7), it may not have yet achieved ideal reaction kinetics at low temperatures. This could be due to reduced activation of catalytic materials, variations in humidity distribution, which affect ionic conductivity and thus operating voltage, and possible variations in gas composition over time due to diffusion phenomena.

The latter can be explained by looking at Membrane Consumption. The increase in membrane consumption at higher temperatures compared to the colder ones may have contributed to the upward trend of the slope.

In order to understand its usefulness and fully determine the consumption of the membrane (or cell components), a deionization filter initially present in the closed water recirculation loop was bypassed.

This allowed impurities, which could originate solely from the cell, to accumulate and increase their concentration over time, based on the cell's consumption rate. Figure 4.8 illustrates what has been described. The effect of temperature on cell consumption is certainly of significant importance as temperatures rise.

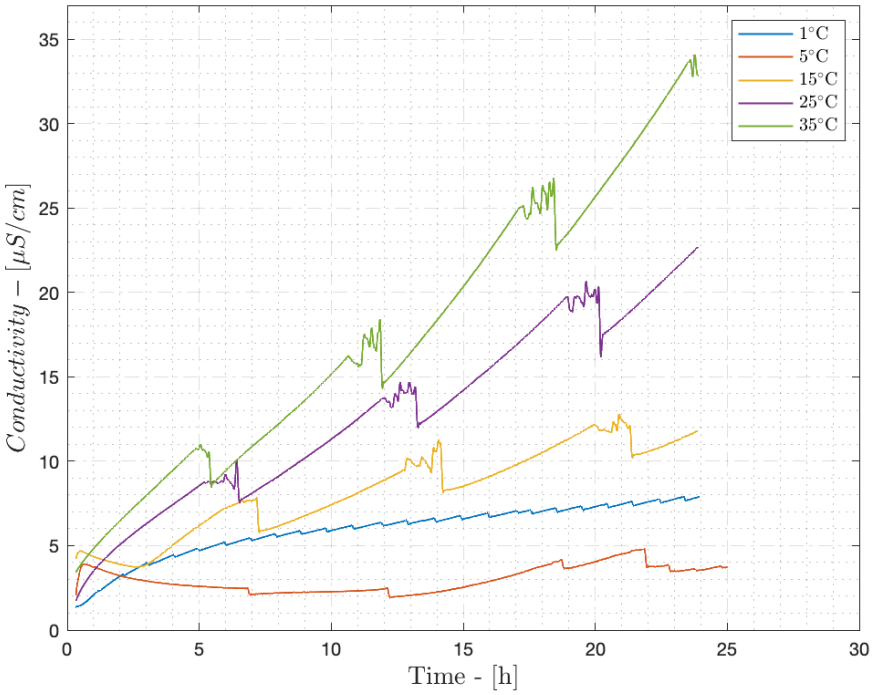

Figure 4.8: H2O Conductivity over Time (failure at $5°C$)

In accordance with what was initially discussed by Chandesris et al. [9] and subsequently further elaborated by Marocco et al. [86], the observed increase in water conductivity is believed to mainly originate from the release of fluorine ions from the membrane. These, by themselves, are not harmful to the extent of poisoning catalytic sites and compromising the proton conductivity of the membrane, as is the case for ions such as Fe^{3+}, Cu^{2+}, Al^{3+}, Mg^{2+}, Ca^{2+} [87, 88]. However, they simultaneously cause an increase in water

conductivity, which, for PEM technology, must be of extreme purity (Deionised, ASTM II, $< 0.1\mu S$) to minimize ohmic losses.

The significant increase in water conductivity is believed to have led to an elevation in operating potential at $35°C$, while at lower temperatures, the effect was negligible within the 24-hour timeframe.

4.5 Gas Analysis

In accordance with Kojima et al. [8] about the importance of recording the quality of the produced hydrogen under different input conditions, the results regarding the influence of an external temperature change on the hydrogen quality are now presented.

Through a series of preliminary tests, the primary atomic masses detected by the Universal Gas Analyzer (UGA) within the generated hydrogen were selected to be recorded. The UGA system uses a two-stage pressure reducing inlet to sample gases at atmospheric pressure. After the pressure is reduced to around 10^{-6} $Torr$, the gas stream is sent to a mass spectrometer (Residual Gas Analyser - RGA) which measures the concentration of each mass of interest.

The graphs below show what has been recorded.

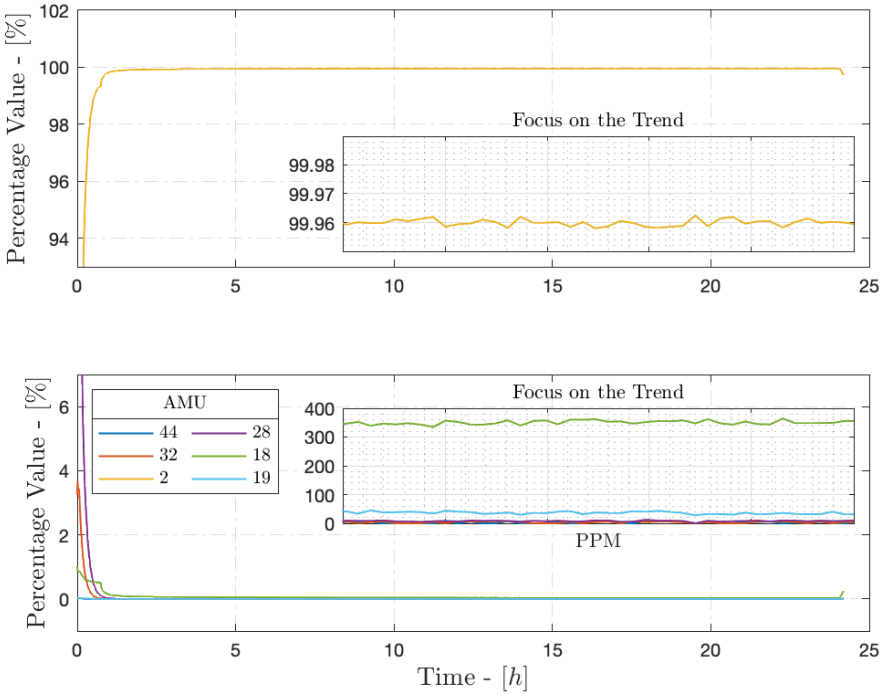

(a) Hydrogen amount of Pollution @ $1°C$

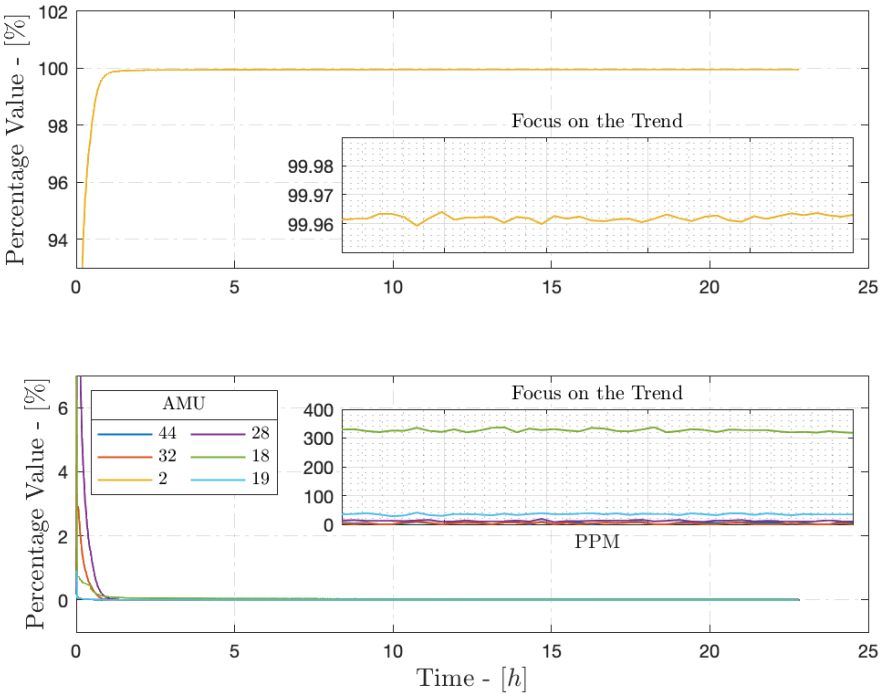

(b) Hydrogen amount of Pollution @ $5°C$

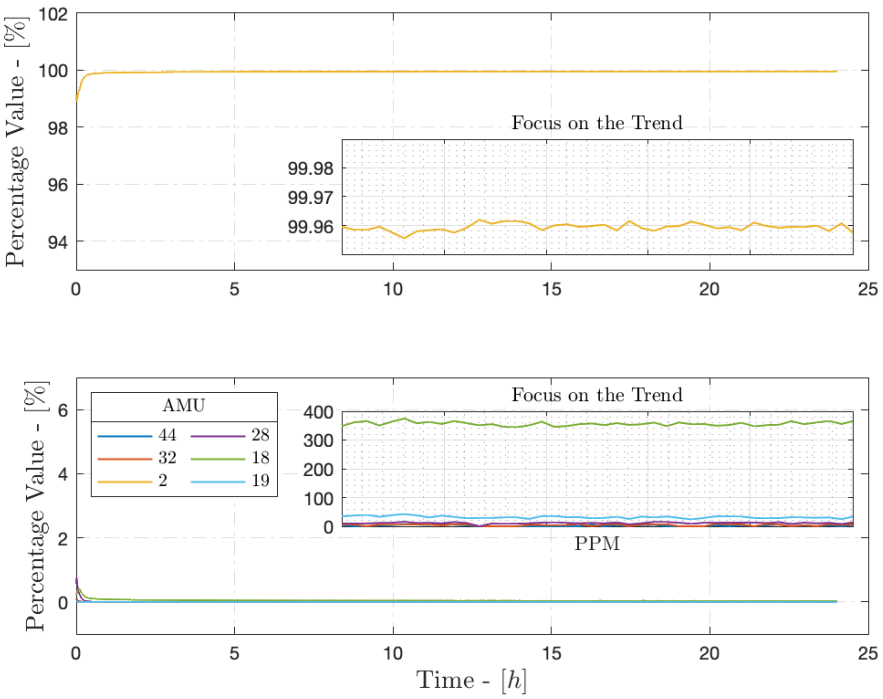

(c) Hydrogen amount of Pollution @ $15°C$

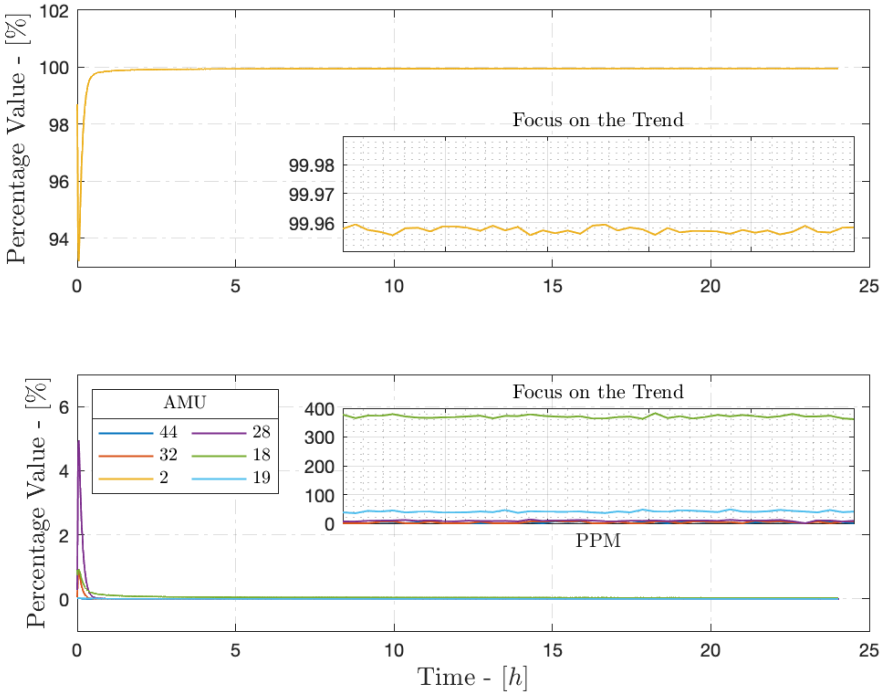

(d) Hydrogen amount of Pollution @ $25°C$

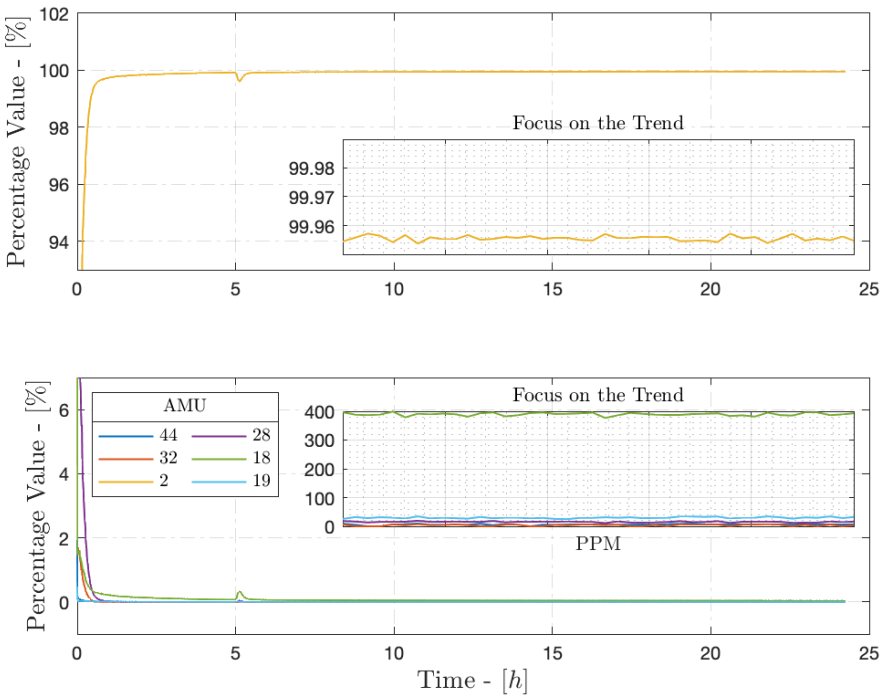

(e) Hydrogen amount of Pollution @ $35°C$

Figure 4.9: Effect of the External Temperature on the Hydrogen Quality, a qualitative result

Based on the graphs in Figure 4.9, some qualitative observations on the interpretation of the detected atomic masses can be made. These in fact do not always reflect the easiest solution.

4.5.1 Atomic Masses: Interpretation and Implications

It should be emphasized that the detected atomic masses cannot be directly associated with specific elements or molecules due to the lack of prior analysis of the sample's composition, such as the water used. Therefore, it is impossible to determine with certainty whether the recorded atomic mass of 19 unified atomic mass units (AMU) corresponds to heavy water (D_2O), fluorine (F), or other potential impurities present in the system.

Referring to the theory underlying the interpretation of mass spectra, it seems more plausible that the peak observed at 19 AMU is associated with isotopes or molecules present in the vicinity of the analyzed process. It is observed that the peak at 18 AMU is likely attributable to residual humidity in the environment, considering that the electrolysis under examination is known to be a wet process. In contrast, it is less likely that this peak represents fluorine (F) since fluorine is an element with significant atomic weight and tends to dissolve in water, as already documented in the scientific literature.

However, the presence of traces of fluorine in the gas production environment is a possibility that should not be entirely disregarded. In this context, it is crucial to highlight the importance of a thorough and accurate investigation to determine its presence.

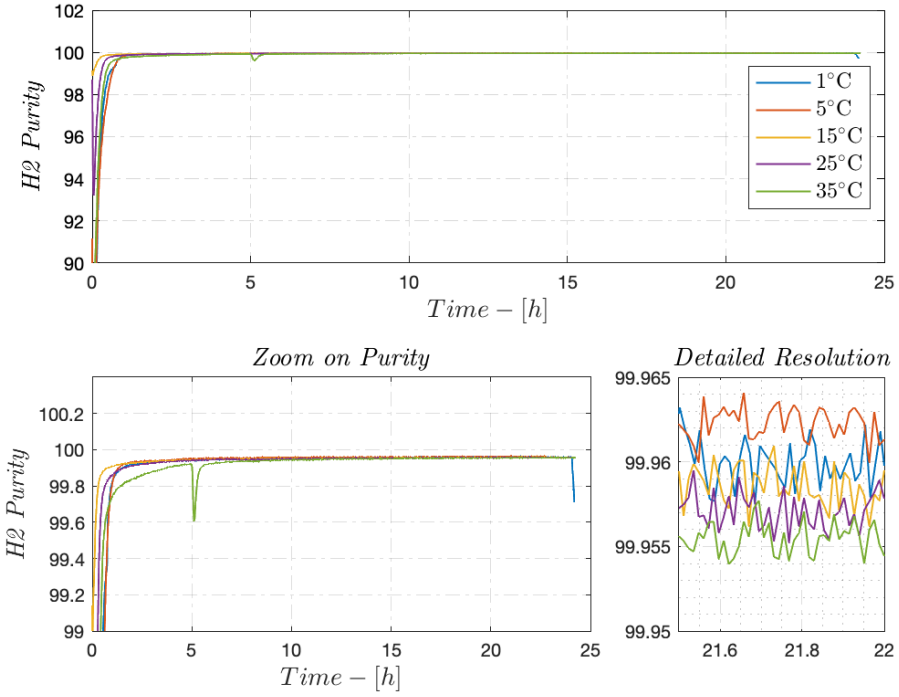

Figure 4.10: Hydrogen quality trends for different external temperatures

Secondly, it should be considered that the detected atomic masses may not be exclusively attributed to the products generated during the electrolysis process. It is essential to note that what was initially analyzed likely represents a residue of the air infiltrated into the system before reaching the desired operating pressure. From that point onward, it can be assumed that everything detected originates exclusively from the electrolytic cell.

However, despite this consideration, atomic masses progressively approaching zero were still included. This approach is justified by the need to understand that during the initial minutes of operation, the produced hydrogen may contain impurities resulting from mixing with external air.

It is important to emphasize that despite these impurities, among the detected components, no critical elements have emerged that could cause severe deterioration or poisoning of a PEM fuel cell if the hydrogen were directly used as input for such a device [89].

The only value that shows a significant variation in response to temperature fluctuations is closely associated with residual humidity, which is the presence of water. It is important to note that residual humidity cannot be categorized as a pollutant; on the contrary, humid hydrogen can even enhance the efficiency of a PEM fuel cell [90]. If, on the other hand, the hydrogen produced is to be stored i.e. under pressure, the residual moisture can be easily extracted by optimising the efficiency of the phase separator or by using subsequent dehumidification steps such as the PSA.

The increasing value observed with rising temperature can be interpreted as a direct consequence of the gas's increased ability to retain water under changing thermal conditions, without representing any significant change in the chemical composition or quality of the gas in question.

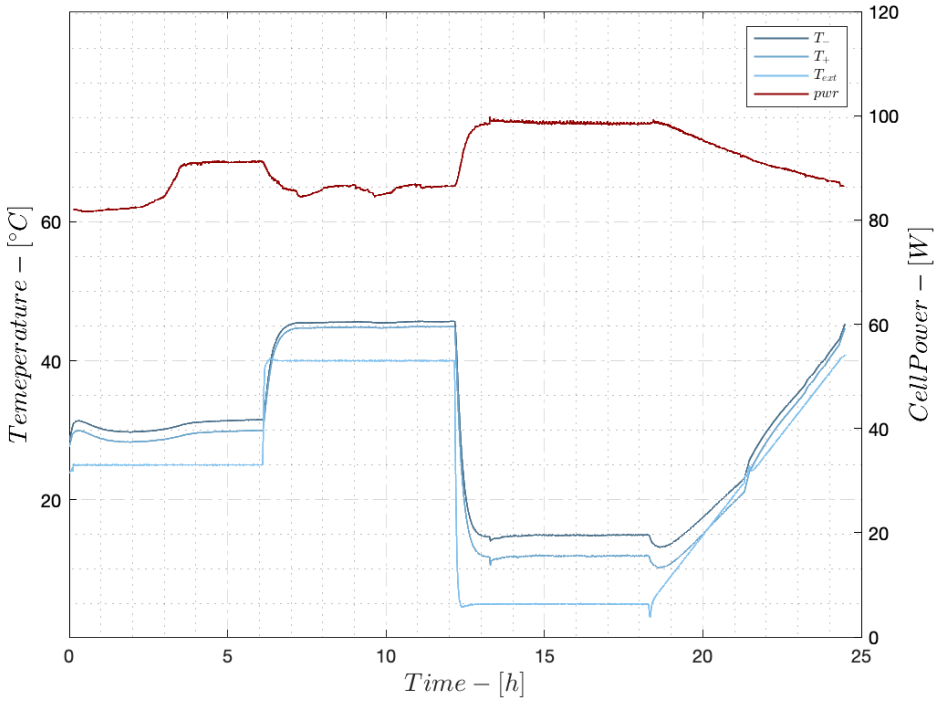

Figure 4.11: Temperature Profile Test

As mentioned in the introduction, despite a change in operating temperature, traces of oxygen crossover were expected. However, this was not detected except at the initial moments, as discussed earlier. In a subsequent analysis involving a variable temperature profile (Figure 4.11), it's evident that the cell effectively tracks the temperature variations

with exceptional responsiveness, but regarding the crossover question, the same results were obtained.

There could be two explanations for this. The first one concerns the physical distance between the cell and the Universal Gas Analyzer (UGA). Due to space constraints and operating temperatures, the UGA could not be placed inside the furnace, and a conduit that carried a portion of the gas outside was necessary. This might have allowed for recombination of oxygen with hydrogen, dilution to the point of being undetectable, or most of it may have followed the gas flow outward without passing through the analyzer.

The second explanation is that, aware of the fact that PEM electrolyzers produce hydrogen of extremely high purity, it is noteworthy that, within the context of the analysis conducted solely with a phase separator preceding the spectrometric analysis, the achieved purity levels (as illustrated in Figure 4.10) consistently remain above 99.9 %. However, it is important to highlight that these purity levels are only achieved after a continuous operation period of at least 5 hours. During this time, in most tests, a thermal and kinetic/chemical equilibrium could be observed.

As a result, for a system powered by intermittent energy sources, where most operational periods are likely to fall within the analyzed temperature ranges, the phase separator alone plays a crucial role. Nevertheless, to ensure a constant maximum quality of the produced hydrogen, the use of auxiliary devices becomes desirable. It is important to emphasize that these devices, willingly or unwillingly, require a minimal input of energy for their operation.

Chapter 5

Conclusion and Remarks

In this work the influences of the external temperature on the operation of a PEM electrolyzer has been studied. Based on the conducted analysis, it can be stated that even a significant variation in external temperature, and consequently, operating temperature, does not seem to have a considerable impact on the quality of the produced hydrogen.

The only changes noted mainly concern: the increase in the amount of residual moisture as the external temperature rises, in traces however small, and the presence of an atomic mass of AMU 19 which, as previously explained, is more likely to be associated with a water molecule consisting of the isotopes of the elements involved.

However, the idea that the minimally detected moisture could be, in part, a recombination of cross over oxygen with hydrogen should not be discarded, hence this phenomenon requires further investigation.

It should also be pointed out that the cell had only been in use for a few hundred hours, so probably, despite operating at high potential and being subject to deterioration at a much faster rate, it had not reached a level of wear and tear that would have released higher quantities of pollutants into the hydrogen. A factor that may have influenced data collection may have been the distance between the cell and the gas analyser. Probably a more compact setup could show variations, albeit slight, in the data collected.

The real significant variation could therefore mainly result only from changes in the input power to the cell, especially if such a variation were of considerable magnitude. This in fact causes transport and diffusion phenomena that temperature variation alone does not cause in the same way.

Considerations on the efficiency of the cell and the overall system have been analyzed. Specifically, it is noted that the efficiency of the entire system is only marginally affected by external temperature ($3 - 4$ %) due to the energy consumption of the auxiliaries, which characterizes the total energy expenditure (relatively constant). On the other hand, the cell's efficiency is significantly affected by temperature ($\simeq 10$ %), causing it to operate at extremely high potentials.

As already mentioned, it is crucial to emphasize that higher temperatures led to an increase in membrane deterioration. While this outcome was expected to some extent, it

was anticipated to be less significant. It is true that the current density applied is not considered high in the literature, and it is known that lower current densities result in a greater release of fluoride ions. However, it is equally true that for the specific cell under examination, such a current density should be regarded as high due to the potentials reached during operation. It should not be discounted that the intermittency (distinct from variability) of the conducted tests, characterized by discontinuous operations, may have contributed to augmenting this trend.

It is crucial to emphasize the key role played by the phase separator in determining the need for additional gas purification systems. If the produced hydrogen is not intended for uses like transportation fuel or laboratory applications requiring maximum purity (in the range of $5.0 - 7.0$), simpler and sometimes passive systems could successfully replace the PSA, thus reducing costs and energy consumption.

Furthermore, uncontrolled start-up, i.e., not regulated to ensure rapid attainment of the operating temperature, as reported in the scientific literature, should be avoided. This practice, especially for larger electrolyzers, may require a significant period to reach the desired operating temperature. However, it is important to note that such thermal controls (potentiostatic, galvanometric or an external heater) can be energetically costly. Based on the above, the trade-off between maintaining the desired operating temperature and operating the electrolyzer in an uncontrolled manner should be carefully evaluated. In some cases, according to the efficiency, it might be more advantageous to allow the cell to operate at a free temperature, as long as it remains below the maximum allowable temperature.

For future analyses, it is strongly recommended to position gas quality detection sensors as close to the cell as possible. Additionally, repeating the study using intermittent energy input would be desirable to more thoroughly assess variations in efficiency and the effects of factors influencing the quality of the produced hydrogen.

Appendix A

A.1 OER Adsorption Step

OER in acidic media

(i) Electrochemical oxide path

$$^{*} + H_2O \rightarrow {}^{*}OH + H^{+} + e^{-} \tag{A.1a}$$

$$^{*}OH \rightarrow {}^{*}O + H^{+} + e^{-} \tag{A.1b}$$

$$^{*}O + H_2O \rightarrow OOH^{*} + H^{+} + e^{-} \tag{A.1c}$$

$$^{*}O_2 \rightarrow {}^{*} + O_2 \tag{A.1d}$$

(ii) Oxide path

$$^{*} + H_2O \rightarrow {}^{*}OH + H^{+}_{(aq)} + e^{-} \tag{A.2a}$$

$$^{*}OH \rightarrow {}^{*}O + {}^{*} + H_2O \tag{A.2b}$$

$$2\,{}^{*}O \rightarrow 2^{*} + O_{2(g)} \tag{A.2c}$$

(iii) Krasil' Shchkov path

$$^{*} + H_2O \rightarrow {}^{*}OH + H^{+}_{(aq)} + e^{-} \tag{A.3a}$$

$$^{*}OH \rightarrow S{-}O^{-} + H^{+}_{(aq)} \tag{A.3b}$$

$$^{*}O^{-} \rightarrow {}^{*}O + e^{-} \tag{A.3c}$$

$$2\,{}^{*}O \rightarrow 2^{*} + O_{2(g)} \tag{A.3d}$$

(iv) Wade and Hackerman's path

$$2^* + 2\,H_2O \rightarrow {}^*O + {}^*H_2O + 2\,H^+_{(aq)} + 2e^- \tag{A.4a}$$

$${}^*O + 2\,{}^*OH^- \rightarrow {}^*H_2O + 2^* + O_{2(g)} + 2e^- \tag{A.4b}$$

OER in basic media

(i) Electrochemical oxide path

$$^* + OH^- \rightarrow {}^*OH + e^- \tag{A.5a}$$

$${}^*OH + OH^-_{(aq)} \rightarrow {}^*O + H_2O + e^- \tag{A.5b}$$

$$2\,{}^*O \rightarrow 2^* + O_{2(g)} \tag{A.5c}$$

(ii) Oxide path

$$^* + OH^-_{(aq)} \rightarrow {}^*OH + e^- \tag{A.6a}$$

$$2\,{}^*OH + OH^-_{(aq)} \rightarrow {}^*O + H_2O \tag{A.6b}$$

$$2\,{}^*O \rightarrow 2^* + O_{2(g)} \tag{A.6c}$$

(iii) Krasil' Shchkov path

$$^* + OH^-_{(aq)} \rightarrow {}^*OH + e^- \tag{A.7a}$$

$${}^*OH + OH^-_{(aq)} \rightarrow {}^*O^- + H_2O \tag{A.7b}$$

$${}^*O^- \rightarrow {}^*O + e^- \tag{A.7c}$$

$${}^*O + {}^*O \rightarrow 2^* + O_{2(g)} \tag{A.7d}$$

(iv) Yeager's path

$$^* + OH^-_{(aq)} \rightarrow {}^*OH + e^- \tag{A.8a}$$

$${}^{*z}OH \rightarrow {}^{*z+1}OH + {}^* + e^- \tag{A.8b}$$

$$2\,{}^{*z+1}OH + 2\,OH^-_{(aq)} \rightarrow 2^* + 2\,H_2O + O_{2(g)} \tag{A.8c}$$

(iv) Bockris path

$$^{*} + OH^{-}_{(aq)} \rightarrow {}^{*}OH + e^{-} \tag{A.9a}$$

$$^{*}OH + OH^{-}_{(aq)} \rightarrow {}^{*}H_2O_2 + e^{-} \tag{A.9b}$$

$$^{*}H_2O_2 + OH^{-}_{(aq)} \rightarrow {}^{*}OOH^{-} + H_2O \tag{A.9c}$$

$$^{*}H_2O_2 + {}^{*}OOH^{-} \rightarrow 2^{*} + OH^{-}_{(aq)} + O_{2(g)} \tag{A.9d}$$

A.2 Step Test

Table A.1: Polarisation curve set points for method B (galvanostatic control)

Set point K^*	**Current density** A/cm^2	**Applied current** A	**Step Duration**
1	0.001	0.06	d
2	0.005	0.32	d
3	0.010	0.64	d
4	0.025	1.59	d
5	0.050	3.18	d
6	0.075	4.77	d
7	0.100	6.36	d
8	0.150	9.54	d
9	0.200	12.72	d
10	0.250	15.9	d
11	0.300	19.08	d
12	0.350	22.26	d
13	0.400	25.44	d
14	0.450	28.62	d
15	0.500	31.80	d
16	0.600	38.16	d
17	0.700	44.52	d
18	0.800	50.88	d
19	0.900	57.24	d
20	1.000	63.61	d
21	1.100	69.96	d
22	1.200	76.32	d
23	1.300	82.68	d
24	1.400	89.04	d
25	1.500	95.40	d
26	1.600	101.76	d

Continued on next page

Table A.1 – continued from previous page

Set point K^*	**Current density** A/cm^2	**Applied current** A	**Step Duration**
27	1.700	108.12	d
28	1.800	114.48	d
29	1.900	120.84	d
30	2.000	127.22	d

Bibliography

[1] *(EI) Statistical Review of Wolrd Energy 2023, (72nd edition)*. URL: https://www.energyinst.org/statistical-review.

[2] *A European strategic long-term vision for a prosperous, modern, competitive and climate neutral economy - doc. n. 52018DC0773*. URL: https://eur-lex.europa.eu/homepage.html.

[3] Carolyn C. Elam et al. "Realizing the hydrogen future: the International Energy Agency's efforts to advance hydrogen energy technologies". In: *International Journal of Hydrogen Energy* 28.6 (2003), pp. 601–607.

[4] Michael Ball and Martin Wietschel. "The future of hydrogen – opportunities and challenges". In: *International Journal of Hydrogen Energy* 34.2 (2009), pp. 615–627.

[5] Frano Barbir. "PEM electrolysis for production of hydrogen from renewable energy sources". In: *Solar Energy* 78.5 (2005), pp. 661–669.

[6] Christoph Rakousky et al. "An analysis of degradation phenomena in polymer electrolyte membrane water electrolysis". In: *Journal of Power Sources* 326 (2016), pp. 120–128.

[7] Shucheng Sun et al. "Investigations on degradation of the long-term proton exchange membrane water electrolysis stack". In: *Journal of Power Sources* 267 (2014), pp. 515–520.

[8] Hirokazu Kojima et al. "Influence of renewable energy power fluctuations on water electrolysis for green hydrogen production". In: *International Journal of Hydrogen Energy* 48.12 (2023), pp. 4572–4593.

[9] M. Chandesris et al. "Membrane degradation in PEM water electrolyzer: Numerical modeling and experimental evidence of the influence of temperature and current density". In: *International Journal of Hydrogen Energy* 40.3 (2015), pp. 1353–1366.

[10] F. Fouda-Onana et al. "Investigation on the degradation of MEAs for PEM water electrolysers part I: Effects of testing conditions on MEA performances and membrane properties". In: *International Journal of Hydrogen Energy* 41.38 (2016), pp. 16627–16636.

[11] M. Anvari et al. "Short term fluctuations of wind and solar power systems". In: *New Journal of Physics* 18.6 (2016).

[12] Alfredo Ursúa et al. “Stand-alone operation of an alkaline water electrolyser fed by wind and photovoltaic systems”. In: *International Journal of Hydrogen Energy* 38.35 (2013), pp. 14952–14967. ISSN: 0360-3199.

[13] Mónica Sánchez et al. “Semi-empirical model and experimental validation for the performance evaluation of a 15 kW alkaline water electrolyzer”. In: *International Journal of Hydrogen Energy* 43.45 (2018), pp. 20332–20345.

[14] Long Phan Van, Long Hieu Hoang, and Tuyen Nguyen Duc. “A comprehensive review of direct coupled photovoltaic-electrolyser system: Sizing techniques, operating strategies, research progress, current challenges, and future recommendations”. In: *International Journal of Hydrogen Energy* 48.65 (2023), pp. 25231–25249.

[15] Eveline Kuhnert, Viktor Hacker, and Merit Bodner. “A Review of Accelerated Stress Tests for Enhancing MEA Durability in PEM Water Electrolysis Cells”. In: *International Journal of Energy Research* 2023 (Feb. 2023). ISSN: 1099-114X.

[16] Andrej Zvonimir Tomić, Ivan Pivac, and Frano Barbir. “A review of testing procedures for proton exchange membrane electrolyzer degradation”. In: *Journal of Power Sources* 557 (2023), p. 232569.

[17] Farid Sayedin et al. “Optimization of Photovoltaic Electrolyzer Hybrid systems; taking into account the effect of climate conditions”. In: *Energy Conversion and Management* 118 (2016), pp. 438–449.

[18] Ozcan Atlam, Frano Barbir, and Dario Bezmalinovic. “A method for optimal sizing of an electrolyzer directly connected to a PV module”. In: *International Journal of Hydrogen Energy* 36.12 (2011), pp. 7012–7018.

[19] A. Khalilnejad, A. Abbaspour, and A.I. Sarwat. “Multi-level optimization approach for directly coupled photovoltaic-electrolyser system”. In: *International Journal of Hydrogen Energy* 41.28 (2016), pp. 11884–11894.

[20] Zhimin Yang, Guangping Zhang, and Bihong Lin. “Performance evaluation and optimum analysis of a photovoltaic-driven electrolyzer system for hydrogen production”. In: *International Journal of Hydrogen Energy* 40.8 (2015), pp. 3170–3179.

[21] Tuyen Nguyen Duc et al. “Optimization strategy for high efficiency 20 kW-class direct coupled photovoltaic-electrolyzer system based on experiment data”. In: *International Journal of Hydrogen Energy* 44.49 (2019), pp. 26741–26752.

[22] “Front Matter”. In: *Fuel Cell Fundamentals*. John Wiley Sons, Ltd, 2016. ISBN: 9781119191766. DOI: https://doi.org/10.1002/9781119191766.fmatter.

[23] Ömer F. Selamet et al. “Effects of operating parameters on the performance of a high-pressure proton exchange membrane electrolyzer”. In: *International Journal of Energy Research* 37.5 (2013), pp. 457–467.

[24] Albert Albert et al. “Stability and Degradation Mechanisms of Radiation-Grafted Polymer Electrolyte Membranes for Water Electrolysis”. In: *ACS Applied Materials & Interfaces* 8.24 (2016), pp. 15297–15306.

[25] Anthony Laconti et al. “Polymer Electrolyte Membrane Degradation Mechanisms in Fuel Cells - Findings Over the Past 30 Years and Comparison with Electrolyzers”. In: *ECS Transactions* 1.8 (2006), p. 199.

[26] Jian Dang et al. “Hydrogen crossover measurement and durability assessment of high-pressure proton exchange membrane electrolyzer”. In: *Journal of Power Sources* 563 (2023), p. 232776.

[27] P. Trinke, B. Bensmann, and R. Hanke-Rauschenbach. “Experimental evidence of increasing oxygen crossover with increasing current density during PEM water electrolysis”. In: *Electrochemistry Communications* (2017).

[28] Agate Martin et al. “On the Correlation between the Oxygen in Hydrogen Content and the Catalytic Activity of Cathode Catalysts in PEM Water Electrolysis”. In: (2021), p. 114513.

[29] Philipp Lettenmeier et al. “Proton Exchange Membrane Electrolyzer Systems Operating Dynamically at High Current Densities”. In: *ECS Transactions* 72.23 (Aug. 2016), p. 11.

[30] V.A. Martinez Lopez et al. “Dynamic operation of water electrolyzers: A review for applications in photovoltaic systems integration”. In: *Renewable and Sustainable Energy Reviews* 182 (2023), p. 113407.

[31] Stefania Siracusano et al. “Analysis of performance degradation during steady-state and load-thermal cycles of proton exchange membrane water electrolysis cells”. In: *Journal of Power Sources* 468 (2020), p. 228390.

[32] Andreas Züttel et al. “Properties of Hydrogen”. In: *Hydrogen as a Future Energy Carrier*. John Wiley Sons, Ltd, 2008. DOI: https://doi.org/10.1002/9783527622894.ch4.

[33] “Front Matter”. In: *Hydrogen Production Technologies*. John Wiley Sons, Ltd, 2017, pp. i–xviii. ISBN: 9781119283676. DOI: https://doi.org/10.1002/9781119283676.fmatter. eprint: https://onlinelibrary.wiley.com/doi/pdf/10.1002/9781119283676.fmatter. URL: https://onlinelibrary.wiley.com/doi/abs/10.1002/9781119283676.fmatter.

[34] C.E.G. Padró and F. Lau. *Advances in Hydrogen Energy*. Springer US, 2013. URL: https://books.google.it/books?id=-GwMswEACAAJ.

[35] Thomas Jordan. “Chapter 2 - Hydrogen technologies”. In: *Hydrogen Safety for Energy Applications*. Ed. by Alexei Kotchourko and Thomas Jordan. Butterworth-Heinemann, 2022.

[36] Bahman Zohuri. *Hydrogen Energy: Challenges and Solutions for a Cleaner Future*. 2018. ISBN: 978-3319934600.

[37] Ali Keçebaş and Muhammet Kayfeci. "Hydrogen properties". In: *Solar Hydrogen Production*. Ed. by Francesco Calise et al. Academic Press, 2019.

[38] Sema Z. Baykara. "Hydrogen: A brief overview on its sources, production and environmental impact". In: *International Journal of Hydrogen Energy* (2018).

[39] *Global Hydrogen Review 2022*. URL: `https://www.iea.org/reports/global-hydrogen-review-2022`.

[40] Canan Acar and Ibrahim Dincer. "Comparative assessment of hydrogen production methods from renewable and non-renewable sources". In: *International Journal of Hydrogen Energy* 39.1 (2014), pp. 1–12.

[41] *2022 Fuel Cell and Hydrogen Observatory (FCHO) Report*. URL: `https://www.fchobservatory.eu/reports`.

[42] Shengjie Peng. *Electrochemical Hydrogen Production from Water Splitting*. 2023. ISBN: 978-981-99-4467-5.

[43] L. Zhang et al. *Electrochemical Water Electrolysis: Fundamentals and Technologies*. CRC Press, 2020. ISBN: 9780429826047.

[44] *GREEN HYDROGEN COST REDUCTION SCALING UP ELECTROLYSERS to meet the 1.5 deg climate goal*. URL: `https://www.irena.org/-/media/Files/IRENA/Agency/Publication/2020/Dec`.

[45] R. L. Leroy, C. T. Bowen, and D. J. Leroy. "The Thermodynamics of Aqueous Water Electrolysis". In: *Journal of the Electrochemical Society* (1980).

[46] Emiliana Fabbri and Thomas J. Schmidt. "Oxygen Evolution Reaction - The Enigma in Water Electrolysis". In: *ACS Catalysis* (2018).

[47] J. Durst et al. "New insights into the electrochemical hydrogen oxidation and evolution reaction mechanism". In: *Energy Environ. Sci.* 7 (2014), pp. 2255–2260.

[48] Marian Chatenet et al. "Water electrolysis: from textbook knowledge to the latest scientific strategies and industrial developments". In: *Chem. Soc. Rev.* (2022).

[49] Y. Matsumoto and E. Sato. "Electrocatalytic properties of transition metal oxides for oxygen evolution reaction". In: *Materials Chemistry and Physics* (1986).

[50] John O'M. Bockris and Takaaki Otagawa. "The Electrocatalysis of Oxygen Evolution on Perovskites". In: *Journal of The Electrochemical Society* (1984).

[51] Tobias Reier et al. "Electrocatalytic Oxygen Evolution Reaction in Acidic Environments – Reaction Mechanisms and Catalysts". In: *Advanced Energy Materials* (2017).

[52] Giuseppe Mattioli et al. "Reaction Pathways for Oxygen Evolution Promoted by Cobalt Catalyst". In: *Journal of the American Chemical Society* (2013).

[53] Dmitry E. Polyansky et al. “Water Oxidation by a Mononuclear Ruthenium Catalyst: Characterization of the Intermediates”. In: *Journal of the American Chemical Society* (2011).

[54] Timothy R. Cook et al. “Solar Energy Supply and Storage for the Legacy and Nonlegacy Worlds”. In: *Chemical Reviews* (2010).

[55] Amanda C. Garcia et al. “Enhancement of Oxygen Evolution Activity of Nickel Oxyhydroxide by Electrolyte Alkali Cations”. In: *Angewandte Chemie International Edition* (2019).

[56] Yangli Pan et al. “Direct evidence of boosted oxygen evolution over perovskite by enhanced lattice oxygen participation”. In: *Nature Communications* (2020).

[57] J. O’M. Bockris and E. C. Potter. “The Mechanism of the Cathodic Hydrogen Evolution Reaction”. In: *Journal of The Electrochemical Society* (1952).

[58] K. C. Neyerlin et al. “Study of the Exchange Current Density for the Hydrogen Oxidation and Evolution Reactions”. In: *Journal of The Electrochemical Society* (2007).

[59] Hubert A. Gasteiger et al. “Activity benchmarks and requirements for Pt, Pt-alloy, and non-Pt oxygen reduction catalysts for PEMFCs”. In: *Applied Catalysis B: Environmental* (2005).

[60] B. V. Tilak and C.-P. Chen. “Generalized analytical expressions for Tafel slope, reaction order and a.c. impedance for the hydrogen evolution reaction (HER): mechanism of HER on platinum in alkaline media”. In: *Journal of Applied Electrochemistry* (1993).

[61] J.M Jakšić, M.V Vojnović, and N.V Krstajić. “Kinetic analysis of hydrogen evolution at Ni–Mo alloy electrodes”. In: *Electrochimica Acta* (2000).

[62] Sergio Trasatti. “Work function, electronegativity, and electrochemical behaviour of metals: III. Electrolytic hydrogen evolution in acid solutions”. In: *Journal of Electroanalytical Chemistry and Interfacial Electrochemistry* (1972).

[63] Asha Raveendran, Mijun Chandran, and Ragupathy Dhanusuraman. “A comprehensive review on the electrochemical parameters and recent material development of electrochemical water splitting electrocatalysts”. In: *RSC Adv.* (2023).

[64] Sengeni Anantharaj et al. “Recent Trends and Perspectives in Electrochemical Water Splitting with an Emphasis on Sulfide, Selenide, and Phosphide Catalysts of Fe, Co, and Ni: A Review”. In: *ACS Catalysis* (2016).

[65] In: *Fuel Cell Fundamentals*. John Wiley Sons, Ltd, 2016.

[66] Allen J. Bard and Larry R. Faulkner. *Electrochemical Methods: Fundamentals and Applications*. Wiley, 2001.

[67] D.S. Falcão and A.M.F.R. Pinto. “A review on PEM electrolyzer modelling: Guidelines for beginners”. In: *Journal of Cleaner Production* 261 (2020), p. 121184.

[68] Chengxiang Xiang, Kimberly M. Papadantonakis, and Nathan S. Lewis. "Principles and implementations of electrolysis systems for water splitting". In: *Mater. Horiz.* (2016).

[69] Frida H. Roenning et al. "Mass transport limitations in polymer electrolyte water electrolyzers using spatially-resolved current measurement". In: *Journal of Power Sources* 542 (2022).

[70] Isabela C. Man et al. "Universality in Oxygen Evolution Electrocatalysis on Oxide Surfaces". In: *ChemCatChem* (2011).

[71] Dan Tang et al. "State-of-the-art hydrogen generation techniques and storage methods: A critical review". In: *Journal of Energy Storage* (2023).

[72] Philipp Haug, Matthias Koj, and Thomas Turek. "Influence of process conditions on gas purity in alkaline water electrolysis". In: *International Journal of Hydrogen Energy* (2017).

[73] Stefania Marini et al. "Advanced alkaline water electrolysis". In: *Electrochimica Acta* (2012).

[74] Naiying Du et al. "Anion-Exchange Membrane Water Electrolyzers". In: *Chemical Reviews* (2022).

[75] Marcelo Carmo et al. "A comprehensive review on PEM water electrolysis". In: *International Journal of Hydrogen Energy* (2013).

[76] S.A. Grigoriev, V.I. Porembsky, and V.N. Fateev. "Pure hydrogen production by PEM electrolysis for hydrogen energy". In: *International Journal of Hydrogen Energy* 31 (2006).

[77] A.S. Gago et al. "Protective coatings on stainless steel bipolar plates for proton exchange membrane (PEM) electrolysers". In: *Journal of Power Sources* (2016).

[78] P. Millet et al. "Scientific and engineering issues related to PEM technology: Water electrolysers, fuel cells and unitized regenerative systems". In: *International Journal of Hydrogen Energy* 36 (2011).

[79] İrem Fırtına, Sıtkı Güner, and Ayhan Albostan. "Preparation and characterization of membrane electrode assembly (MEA) for PEMFC". In: *International Journal of Energy Research* (2011).

[80] Christoph Immerz et al. "Effect of the MEA design on the performance of PEMWE single cells with different sizes". In: *Journal of Applied Electrochemistry* (2018).

[81] S.A. Grigoriev et al. "Optimization of porous current collectors for PEM water electrolysers". In: *International Journal of Hydrogen Energy* (2009).

[82] Christoph Rakousky et al. "Polymer electrolyte membrane water electrolysis: Restraining degradation in the presence of fluctuating power". In: *Journal of Power Sources* (2017).

[83] Steffen Henrik Frensch et al. “Influence of the operation mode on PEM water electrolysis degradation”. In: *International Journal of Hydrogen Energy* (2019).

[84] Edward Rauls et al. “Favorable Start-Up behavior of polymer electrolyte membrane water electrolyzers”. In: *Applied Energy* (2023).

[85] Malkow T et al. “EU harmonised polarisation curve test method for low-temperature water electrolysis”. In: KJ-NA-29182-EN-N (online),KJ-NA-29182-EN-C (print) (2018).

[86] Paolo Marocco et al. “Online measurements of fluoride ions in proton exchange membrane water electrolysis through ion chromatography”. In: *Journal of Power Sources* (2021).

[87] Na Li et al. “The effects of cationic impurities on the performance of proton exchange membrane water electrolyzer”. In: *Journal of Power Sources* (2020).

[88] Ryoya Yoshimura et al. “Effects of Artificial River Water on PEM Water Electrolysis Performance”. In: *Catalysts* (2022).

[89] B. Shabani et al. “Poisoning of proton exchange membrane fuel cells by contaminants and impurities: Review of mechanisms, effects, and mitigation strategies”. In: *Journal of Power Sources* (2019).

[90] Xi Chen et al. “Temperature and humidity management of PEM fuel cell power system using multi-input and multi-output fuzzy method”. In: *Applied Thermal Engineering* (2022).